Gapped superconductivity with all symmetries in InSb (110) quantum wells in proximity to *s*-wave superconductor in Fulde-Ferrell-Larkin-Ovchinnikov phase or with a supercurrent

F. Yang and M. W. Wu*

Hefei National Laboratory for Physical Sciences at Microscale, Department of Physics, and CAS Key Laboratory of Strongly-Coupled Quantum Matter Physics, University of Science and Technology of China, Hefei, Anhui, 230026, China

(Received 18 November 2016; revised manuscript received 3 January 2017; published 9 February 2017)

We show that all the singlet even-frequency, singlet odd-frequency, triplet even-frequency, and triplet odd-frequency pairings, together with the corresponding order parameters (gaps), can be realized in InSb (110) spin-orbit-coupled quantum well in proximity to *s*-wave superconductor in Fulde-Ferrell-Larkin-Ovchinnikov phase or with a supercurrent. It is revealed that with the singlet even-frequency order parameter induced by the proximity effect, triplet even-frequency pairing is induced due to the broken spin-rotational symmetry by the spin-orbit coupling. Since the translational symmetry is broken by the center-of-mass momentum of Cooper pair in Fulde-Ferrell-Larkin-Ovchinnikov phase or with a supercurrent, the singlet odd-frequency pairing can be induced. With the translational and spin-rotational asymmetries, the triplet odd-frequency pairing is also realized. Then, we show that the corresponding order parameters can be obtained from the self-energy of the electron-electron Coulomb interaction with the dynamic screening. The singlet and the induced triplet even-frequency order parameters are found to exhibit the conventional *s*- and *p*-wave characters in the momentum space, respectively. Whereas for the induced odd-frequency order parameters in quantum well, the singlet and triplet ones show the *p*- and *d*-wave characters, respectively. Moreover, the *p*-wave character of the singlet odd-frequency order parameter exhibits anisotropy with respect to the direction of the center-of-mass momentum. While for the triplet one, we find that d_{x^2}- and d_{xy}-wave characters can be obtained with respect to the direction of the center-of-mass momentum. We show that at proper density, the singlet even-frequency order parameter is suppressed and the induced singlet odd-frequency, triplet even-frequency, and triplet odd-frequency ones can be detected experimentally.

DOI: 10.1103/PhysRevB.95.075304

I. INTRODUCTION

In the field of superconductivity, symmetry of the Cooper-pair wave function in spin, time, and orbital spaces has attracted much attention for the past few decades. Within the framework of superconductivity theory developed by Bardeen, Cooper, and Schrieffer (BCS) [1], it is established that a Cooper pair is formed by two electrons with momenta $\mathbf{q}+\mathbf{k}$ and $\mathbf{q}-\mathbf{k}$ near the Fermi surface. Due to the Fermi-Dirac statistics, the Cooper-pair wave function must have sign change in the exchange of the two electrons. In the spin space, Cooper pair can be classified into either singlet or triplet type. As for the orbital part of the pair wave function, when we focus on the symmetry with respect to the exchange of two momenta $\mathbf{q}+\mathbf{k}$ and $\mathbf{q}-\mathbf{k}$, i.e., $\mathbf{k}\rightarrow-\mathbf{k}$, one can define the parity of the Cooper pair. For the conventional BCS superconductors such as Al, Pb, and Nb, in the presence of the translational symmetry ($\mathbf{q}=0$) and together with the space, time-inversion, and spin-rotational symmetries, the Cooper pairs are in the singlet even-frequency even-parity state, in accord with the Fermi-Dirac statistics. Here, even/odd frequency refers to the situation that the pair wave function is even/odd with respect to the exchange of time coordinates.

In 1974, Berezinskii considered the possibility of the triplet even-frequency pairing with even parity in the observed phase of ^{3}He [2]. After that, the possibilities of the Cooper pair with other symmetries are extensively studied, and from the symmetry analysis [3], Cooper pairs can be classified into (i) singlet even frequency (SE) with even parity; (ii) singlet odd frequency (SO) with odd parity; (iii) triplet odd frequency (TO) with even parity; (iv) triplet even frequency (TE) with odd parity. Specifically, after the proposal by Berezinskii, TO pairing has been discussed in a wide variety of theoretical models with spin-rotational and time-inversion asymmetries [4–11], e.g., Kondo model [4,6], Hubbard model [5,7,9,10], and heavy-fermion system [8,11]. Meanwhile, several proposals about the SO pairing have also been reported in the inhomogeneous systems with space- and time-inversion asymmetries by introducing effective *p*-wave electron-electron (e-e) interaction [12–16]. In the presence of the odd-frequency pairings, by considering the retardation effect of the electron interaction, odd-frequency gaps or odd-frequency order parameters are theoretically suggested [11,13,15,17]. However, up until now, odd-frequency bulk superconductor has not yet been realized experimentally. Moreover, it is now commonly believed that the pairing in superfluid ^{3}He is in the TE type [18–25]. Recently, much effort has been focused on the superconductivity in material Sr_2RuO_4 due to the generally recognized similarity to that in ^{3}He [26–36]. The pairing and order parameter in superconducting Sr_2RuO_4 are theoretically suggested [26–28,30] and primarily confirmed from recent experiments [29,31–36] to be the *p*-wave TE type. Furthermore, it is reported very recently that the TE pairing and order parameter can also be realized in the noncentrosymmetric superconductor [37–39] with spin-orbit coupling (SOC) existing in nature [40–42], whose experimental confirmations are still in progress.

Although it is not easy so far to realize odd-frequency superconductivity and/or triplet one in the uniform bulk system, it is more promising to induce these pairings in the

*Author to whom correspondence should be addressed: mwwu@ustc.edu.cn

inhomogeneous systems with lower symmetry. Specifically, in the last decade, the proximity effect has been studied intensively in multilayered structures consisting of superconductors and nonsuperconducting systems and it is well known that the superconducting correlation can penetrate into the normal region. In superconductor-ferromagnet structure, with the time-inversion and spin-rotational asymmetries, it is well established that the TO pairing is induced in ferromagnet [43–51]. Moreover, it was predicted that with the inhomogeneous ferromagnet, the induced TO pairing can diffuse into the ferromagnet with the longer diffusion length than that of the SE one [43]. Nevertheless, with the conventional s-wave electron-electron (e-e) interaction, the TO gap (i.e., the TO order parameter) is zero. Similar to the magnetization, the SOC can also break the spin-rotational symmetry. Together with the broken space-inversion symmetry by the SOC, the TE pairing is expected to be induced [52–58], which was first pointed out by Gor'kov and Rashba in s-wave superconductor with the SOC induced by the absorption of ion [52]. Then, a great deal of efforts have been devoted to the multilayered structures consisting of superconductors and spin-orbit-coupled nonsuperconducting systems as a natural extension [53–58]. The induced TE pairing is further proved to possess parallel spin projection to the effective magnetic field due to the SOC [52,54–58]. However, even in the presence of the TE pairing, with the momentum-independent s-wave e-e interaction, no TE gap (TE order parameter) is realized. Nevertheless, de Gennes pointed out that in the nonsuperconducting material proximity to superconductor, the pairing penetrating from superconductor experiences the many-body interaction [59], and hence order parameter can be induced even with a repulsive effective e-e interaction. Following the work by de Gennes [59], it is reported by Yu and Wu very recently that the TE order parameter is induced in the spin-orbit coupled quantum well (QW) in proximity to s-wave superconductor [58]. Specifically, with the induced TE pairing in QW by the SOC, they showed that from the self-energy of the e-e Coulomb interaction, the TE order parameter can be induced.

Except for the multilayered structures, the study of the mixed types of Cooper pairs in superconductors with vortex structure, where the translational symmetry is broken, has a long history [60–69]. It is known that due to the translational asymmetry, the SO pairing is induced near the vortex core [3,60–69]. Aside from the vortex structure, the translational symmetry can also be broken by a supercurrent in superconductors, which leads to the center-of-mass (c.m.) momentum of the Cooper pair, as revealed both experimentally [70] and theoretically [71] in recent works. Moreover, except for the extrinsic breakdown of the translational symmetry above, there exists a high-magnetic-field phase in the superconductor, referred as Fulde-Ferrell-Larkin-Ovchinnikov (FFLO) phase [72,73], where the translational symmetry is spontaneously broken by inducing the c.m. momentum of the Cooper pair. In the FFLO phase, the Zeeman energy leads to different Fermi surfaces for spin-up and -down electrons, and then by inducing a finite c.m. momentum of the Cooper pair, the pairing region between the spin-up and -down electrons near the Fermi surfaces can be maximized, leading to the free energy minimized. Consequently, there exist pairing electrons and unpairing ones in the FFLO phase. Furthermore, with translational and spin-rotational asymmetries by the magnetic field, all four types of pairings are expected to be induced [74]. Nevertheless, with the conventional symmetric s-wave e-e interaction, only the SE order parameter exists in the FFLO phase. It is natural to consider the possibility to induce and manipulate all four types of order parameters, which may lead to rich physics especially for the quasiparticles. Multilayered structures consisting of nonsuperconducting systems and s-wave superconductors in FFLO phase or with a supercurrent hence naturally come to our attention.

In this work, we show that the order parameters containing all four types of symmetry, i.e., the SE, SO, TE, and TO, can be realized in the two-dimensional electron gas (2DEG) of the spin-orbit-coupled InSb (110) QW [75–79] in proximity to s-wave superconductors in FFLO phase or with a supercurrent. Specifically, the SE order parameter can be induced in QW through the proximity effect. We show that there exist unpairing regions in the momentum space, where the proximity-induced SE order parameter vanishes. It is further revealed that the unpairing regions arise from the FFLO-phase-like blocking in QW. With this proximity-induced SE order parameter, SO (TE) pairing is induced due to the broken translational (spin-rotational) symmetry by the c.m. momentum of Cooper pair (SOC). With the translational and spin-rotational asymmetries, the TO pairing can also be induced. Then, we show that from the self-energy due to the e-e Coulomb interaction with the dynamical screening [80–82], the corresponding order parameters can be induced and the proximity-induced SE order parameter is also renormalized. Particularly, we reveal that the odd-frequency order parameters are induced due to the retardation effect of the Coulomb interaction from the dynamic screening in 2DEG, where the plasmon effect is important. In addition, the induced triplet order parameters are shown to possess parallel spin projections to the effective magnetic field due to the SOC, similar to the previous works [52,54–58].

Differing from the vanishing proximity-induced SE order parameter in the unpairing regions, it is found that through the renormalization due to the e-e Coulomb interaction, the SE, SO, TE, and TO ones in QW all have small strengths in the unpairing regions. Moreover, in the pairing regions, rich behaviors of the order parameters containing all four types of symmetry are revealed. Specifically, the SE order parameter Δ_{SE} exhibits an s-wave behavior in the momentum space, while the induced SO (TE) one Δ_{SO} (Δ_{TE}) shows a p-wave character. Particularly, with the broken translational symmetry by the c.m. momentum of Cooper pair, the p-wave character of the induced SO order parameter shows anisotropy with respect to the direction of the c.m. momentum. This is very different from the TE one, which is determined by the SOC and hence is independent on the direction of c.m. momentum. As for the induced TO order parameter Δ_{TO}, the unconventional d-wave character in the momentum space is revealed and, particularly, when the c.m. momentum is along the $[1\bar{1}0]$ and [001] directions, the d_{x^2}- and d_{xy}-wave characters can be obtained, respectively. This anisotropy of the TO order parameter is further proved to arise from the unique SOC structure in InSb (110) QW. The specific behaviors of the order parameters containing all four types of symmetry are

TABLE I. Order parameters' behaviors in the momentum space. $\Delta_{\rm SE}^{T}$ stands for the proximity-induced SE order parameter. $C_{\rm SE}(k,\omega)$, $C_{\rm SO}(k,\omega)$, $C_{\rm TE}(k,\omega)$, $C_{\rm TO}^{0}(k,\omega)$, and $C_{\rm TO}^{1}(k,\omega)$ are independent on the orientation of the momentum.

Order parameter	Behavior in the momentum space
$\Delta_{\rm SE}$	$\Delta_{\rm SE}^{T}+C_{\rm SE}(k,\omega)$
$\Delta_{\rm SO}$	$C_{\rm SO}(k,\omega)\mathbf{k}\cdot\mathbf{q}$
$\Delta_{\rm TE}$	$C_{\rm TE}(k,\omega)\mathbf{k}\cdot\mathbf{e_x}$
$\Delta_{\rm TO}$	$C_{\rm TO}^{0}(k,\omega)\mathbf{q}\cdot\mathbf{e_x}-C_{\rm TO}^{1}(k,\omega)(\mathbf{k}\cdot\mathbf{e_x})(\mathbf{k}\cdot\mathbf{q})$

summarized in Table I. Furthermore, we show that at proper density, the SE order parameter can be efficiently suppressed through the renormalization from the repulsive e-e Coulomb interaction, as revealed in the previous work [58], and the induced SO, TE, and TO order parameters can be detected and distinguished experimentally.

This paper is organized as follows. In Sec. II, we introduce our model and lay out Hamiltonian. In Sec. III, we present the analytical results including the SE, SO, TE, and TO pairing functions and the calculation of the self-energy due to the e-e Coulomb interaction. The specific numerical results in InSb (110) QW and analytic analysis are presented in Sec. IV. We summarize in Sec. V.

II. MODEL AND HAMILTONIAN

In this section, we present the Hamiltonian of the QW in proximity to s-wave superconductors in FFLO phase or with a supercurrent in the Nambu $\otimes$ spin space, including the QW $\hat{H}_{\rm QW}$ with the growth direction along the $\hat{z}$ axis, the superconductor $\hat{H}_{\rm S}$ in FFLO phase, or with a supercurrent (the c.m. momentum of Cooper pair $\mathbf{q}$ is chosen to be along the in-plane direction), and the tunneling between the QW and superconductor $\hat{H}_{\rm T}$. By defining the Nambu spinors in QW $\hat{\Psi}_{\mathbf{k}}(t)=[\psi_{\uparrow\mathbf{k}+\mathbf{q}}(t),\psi_{\downarrow\mathbf{k}+\mathbf{q}}(t),\psi^{\dagger}_{\uparrow-\mathbf{k}+\mathbf{q}}(t),\psi^{\dagger}_{\downarrow-\mathbf{k}+\mathbf{q}}(t)]^{T}$ and in superconductor $\hat{\Phi}_{\mathbf{p}}(t)=[\phi_{\uparrow\mathbf{p}+\mathbf{q}}(t),\phi_{\downarrow\mathbf{p}+\mathbf{q}}(t),\phi^{\dagger}_{\uparrow-\mathbf{p}+\mathbf{q}}(t),\phi^{\dagger}_{\downarrow-\mathbf{p}+\mathbf{q}}(t)]^{T}$, with $\mathbf{k}=k_x\mathbf{e_x}+k_y\mathbf{e_y}$ and $\mathbf{p}=p_x\mathbf{e_x}+p_y\mathbf{e_y}+p_z\mathbf{e_z}$ being the momenta of the electrons in QW and superconductor, respectively, these Hamiltonians are given in the following.

The Hamiltonian of the spin-orbit-coupled QW is given by [58]

$$\hat{H}_{\rm QW}=\hat{H}^{\rm k}_{\rm QW}+\hat{H}^{\rm SOC}_{\rm QW}+\hat{H}^{\rm ee}_{\rm QW}, \tag{1}$$

where $\hat{H}^{\rm k}_{\rm QW}$, $\hat{H}^{\rm SOC}_{\rm QW}$, and $\hat{H}^{\rm ee}_{\rm QW}$ are the kinetic energy, the SOC, and the e-e Coulomb interaction, respectively:

$$\hat{H}^{\rm k}_{\rm QW}=\frac{1}{2}\int d\mathbf{k}\,\hat{\Psi}^{\dagger}_{\mathbf{k}}(t)\begin{pmatrix}\xi^{c}_{\mathbf{k}+\mathbf{q}} & 0\\ 0 & \xi^{c}_{-\mathbf{k}+\mathbf{q}}\end{pmatrix}\rho_3\hat{\Psi}_{\mathbf{k}}(t), \tag{2}$$

$$\hat{H}^{\rm SOC}_{\rm QW}=\frac{1}{2}\int d\mathbf{k}\,\hat{\Psi}^{\dagger}_{\mathbf{k}}(t)\begin{pmatrix}h_{\mathbf{k}+\mathbf{q}} & 0\\ 0 & h_{-\mathbf{k}+\mathbf{q}}\end{pmatrix}\rho_3\hat{\Psi}_{\mathbf{k}}(t), \tag{3}$$

$$\hat{H}^{\rm ee}_{\rm QW}=\frac{1}{8}\int d\mathbf{k}\,d\mathbf{k}'d\mathbf{q}'V_{\mathbf{q}'}(t-t')[\hat{\Psi}^{\dagger}_{\mathbf{k}+\mathbf{q}'}(t)\rho_3\hat{\Psi}_{\mathbf{k}}(t)]\times[\hat{\Psi}^{\dagger}_{\mathbf{k}'-\mathbf{q}'}(t')\rho_3\hat{\Psi}_{\mathbf{k}'}(t')]. \tag{4}$$

Here, $\xi^{c}_{\mathbf{k}}=\varepsilon^{c}_{\mathbf{k}}-\mu_c$ and $\varepsilon^{c}_{\mathbf{k}}=k^2/(2m^{*}_{c})$ with m^{*}_{c} and μ_c being the effective mass and chemical potential of the electron in QW, respectively; $h_{\mathbf{k}}$ represents the SOC; $\rho_3=\sigma_0\otimes\tau_3$; σ_i and τ_i stand for the Pauli matrices in spin and particle-hole spaces, respectively. The e-e Coulomb interaction with the dynamic screening considered is given by $V_{\mathbf{k}}(t-t')=\int d\omega\, e^{-i\omega(t-t')}V_{\mathbf{k}}(\omega)$ with

$$V_{\mathbf{k}}(\omega)=\frac{V^{0}_{\mathbf{k}}}{\epsilon(\mathbf{k},\omega)}. \tag{5}$$

Here, $V^{0}_{\mathbf{k}}=2\pi e^2/(\epsilon_0\kappa_0 q)$ stands for the unscreened Coulomb potential in a two-dimensional (2D) system; ϵ_0 and κ_0 represent the vacuum permittivity and relative dielectric constant, respectively; $\epsilon(\mathbf{q},\omega)$ is the dynamic dielectric function. In the long-wavelength limit ($\omega>qv_F$), based on the linear response theory [80–82], the expression of $V_{\mathbf{k}}(\omega)$ can be given by

$$V_{\mathbf{k}}(\omega)=V^{\rm re}_{\mathbf{k}}+V^{\rm at}_{\mathbf{k}}(\omega), \tag{6}$$

where $V^{\rm re}_{\mathbf{k}}=V^{0}_{\mathbf{k}}$; $V^{\rm at}_{\mathbf{k}}=V^{0}_{\mathbf{k}}|\omega^{pl}_{\mathbf{k}}|^2/(\omega^2-|\omega^{pl}_{\mathbf{k}}|^2)$, which has been revealed in the previous work [83] to act as a retarded attractive potential; $\omega^{pl}_{\mathbf{k}}=\sqrt{2\pi e^2nk/(m^{*}_{c}\epsilon_0\kappa_0)}$ is the plasma frequency with n being the density of the electrons.

The Hamiltonian of the s-wave superconductor in FFLO phase or with a supercurrent is expressed as [72,73]

$$\hat{H}_S=\int\frac{d\mathbf{p}}{2}\hat{\Phi}^{\dagger}_{\mathbf{p}}(t)\begin{pmatrix}\xi^{s}_{\mathbf{p}+\mathbf{q}}+h_B\sigma_z & \Delta_0 i\sigma_2\\ \Delta^{*}_0 i\sigma_2 & \xi^{s}_{-\mathbf{p}+\mathbf{q}}+h_B\sigma_z\end{pmatrix}\rho_3\hat{\Phi}_{\mathbf{p}}(t), \tag{7}$$

where $\xi^{s}_{\mathbf{p}}=\varepsilon^{s}_{\mathbf{p}}-\mu_s$ and $\varepsilon^{s}_{\mathbf{p}}=p^2/(2m^{*}_{c})$ with m^{*}_{s} and μ_s representing the effective mass and chemical potential of the electrons in superconductor, respectively; Δ_0 denotes the singlet gap and h_B stands for the Zeeman energy in the superconductor. In this work, we mainly consider the physics of the translational asymmetry by the c.m. momentum of Cooper pair, which can be induced by either the FFLO phase or a supercurrent in superconductors, as mentioned in the Introduction. The magnetic field in QWs, which can lead to TO pairing in QWs as revealed in the previous works [43–51], is not included here. Particularly, for the case of superconductors in FFLO phase (or with a supercurrent), our proposal can be realized in N/S/F (or N/S) structures, hence, the magnetic field in QWs is not considered.

The tunneling Hamiltonian between the QW and superconductor reads as [58,84–86]

$$\hat{H}_T=\int d\mathbf{k}\,dp_z\big[\Psi^{\dagger}_{\mathbf{k}}(t)t_0\rho_3\Phi_{(\mathbf{k},p_z)}(t)+\Phi^{\dagger}_{(\mathbf{k},p_z)}(t)t^{*}_0\rho_3\Psi_{\mathbf{k}}(t)\big], \tag{8}$$

with t_0 being the tunneling matrix element.

III. ANALYTICAL RESULTS

We first start our investigation from the effective Bogoliubov–de Gennes (BdG) Hamiltonian in InSb (110) QW following the approach in the previous work [58] by using the equilibrium Green functions [80–82], and show that the

singlet and triplet order parameters can be induced from the self-energy due to the e-e Coulomb interaction. In InSb (110) QW, the SOC $h_{\mathbf{k}} = \gamma_D k_x (k_x^2 - 2k_y^2 - \langle k_z^2 \rangle)\sigma_z$, with γ_D being the Dresselhaus coefficient [87]. Particularly, since $\langle k_z^2 \rangle \gg k_F^2$ in QW [75–78], one approximately has

$$h_{\mathbf{k}} = -\gamma_D \langle k_z^2 \rangle k_x \sigma_z. \tag{9}$$

Here, the in-plane coordinate axes are set as $x \parallel [1\bar{1}0]$ and $y \parallel [001]$ with $\mathbf{e_x}$ ($\mathbf{e_y}$) being the unit vector along the $\hat{x}$ ($\hat{y}$) direction. Furthermore, it has been shown in the previous work [58] that in InSb QWs, the self-energy due to the electron-phonon interaction is much smaller than that due to the e-e Coulomb interaction at low temperature, and hence only the Coulomb interaction needs to be considered in this work.

A. Effective BdG Hamiltonian in QW

In the Nambu $\otimes$ spin space, the equilibrium Green function in the momentum space is given by

$$G_{\mathbf{k}}(t) = -i\rho_3 \langle T \hat{\Psi}_{\mathbf{k}}(t) \hat{\Psi}_{\mathbf{k}}^{\dagger}(0) \rangle, \tag{10}$$

where T represents the time-ordering operator; $\langle \ldots \rangle$ denotes the ensemble average. By expressing

$$G_{\mathbf{k}}(t) = \begin{pmatrix} g_{\mathbf{k}}(t) & f_{\mathbf{k}}(t) \\ f_{-\mathbf{k}}^{\dagger}(t) & g^{\dagger}{}_{-\mathbf{k}}(t) \end{pmatrix}, \tag{11}$$

one can obtain the normal Green function $g_{\mathbf{k}}(t)$ and anomalous Green function $f_{\mathbf{k}}(t)$ [52,58,80–82].

In the frequency space $G_{\mathbf{k}}(\omega) = \int_{-\infty}^{\infty} e^{i\omega t} G_{\mathbf{k}}(t)$, the Gor'kov equation [88] in QW is given by

$$\left(\omega\rho_3 - H_{\mathrm{QW}}^{\mathrm{k}} - H_{\mathrm{QW}}^{\mathrm{SOC}}\right) G_{\mathbf{k}}^0(\omega) = 1, \tag{12}$$

with $G_{\mathbf{k}}^0(\omega)$ being the free Green function. When the interaction is considered, from the Dyson equation $G_{\mathbf{k}}(\omega) = G_{\mathbf{k}}^0(\omega) + G_{\mathbf{k}}^0(\omega)\hat{\Sigma}(\mathbf{k},\omega)G_{\mathbf{k}}(\omega)$ [80–82], one obtains

$$\left[\omega\rho_3 - H_{\mathrm{QW}}^{\mathrm{k}} - H_{\mathrm{QW}}^{\mathrm{SOC}} - \hat{\Sigma}(\mathbf{k},\omega)\right] G_{\mathbf{k}}(\omega) = 1, \tag{13}$$

where $\hat{\Sigma}(\mathbf{k},\omega)$ are the self-energies due to H_T and $H_{\mathrm{QW}}^{\mathrm{ee}}$. By comparing Eq. (13) with Eq. (12), the effective BdG Hamiltonian in QW is obtained [58]:

$$\hat{H}_{\mathrm{QW}}^{\mathrm{BdG}} = \hat{H}_{\mathrm{QW}}^{0} + \hat{\Sigma}(\mathbf{k},\omega), \tag{14}$$

from which one can obtain the singlet and triplet order parameters and calculate the energy spectra of the elementary excitation.

B. Self-energy due to the proximity effect

Following the previous work [58], by approximately considering that the e-e Coulomb interaction is weaker than the proximity effect, we first calculate the self-energy due to the proximity effect without the e-e Coulomb interaction to determine the Green function, and then obtain the self-energy due to the e-e Coulomb interaction.

The self-energy due to the tunneling is calculated based on Hamiltonian (8), written as

$$\hat{\Sigma}_T(\mathbf{k},\omega) = |t_0|^2 \int dp_z G_{\mathbf{k}+p_z\mathbf{e_z}}^{s}(\omega). \tag{15}$$

Here, $G_{\mathbf{p}}^{s}(\omega) = \int_{-\infty}^{\infty} e^{i\omega t} G_{\mathbf{p}}^{s}(t)$ with $G_{\mathbf{p}}^{s}(t)$ being the Green function in superconductor, written as

$$G_{\mathbf{p}}^{s}(t) = -i\rho_3 \langle T \hat{\Phi}_{\mathbf{p}}(t) \hat{\Phi}_{\mathbf{p}}^{\dagger}(0) \rangle = \begin{pmatrix} g_{\mathbf{p}}^{s}(t) & f_{\mathbf{p}}^{s}(t) \\ f^{s\dagger}{}_{-\mathbf{p}}(t) & g^{s\dagger}{}_{-\mathbf{p}}(t) \end{pmatrix}. \tag{16}$$

$g_{\mathbf{p}}^{s}(t)$ and $f_{\mathbf{p}}^{s}(t)$ are the normal and anomalous Green functions, respectively. Specifically, in the frequency space, the anomalous Green function is given by

$$f_{\mathbf{p}}^{s}(\omega) = \begin{pmatrix} 0 & \dfrac{\Delta_0}{D_{\mathbf{p},\omega}(h_B)} \\ \dfrac{-\Delta_0}{D_{\mathbf{p},\omega}(-h_B)} & 0 \end{pmatrix}, \tag{17}$$

where $D_{\mathbf{p},\omega}(\pm h_B) = (\omega - \xi_{\mathbf{p}+\mathbf{q}}^{s} \mp h_B)(-\omega - \xi_{\mathbf{p}-\mathbf{q}}^{s} \pm h_B) + |\Delta_0|^2$. By neglecting the diagonal terms in Eq. (15) which are marginal at the weak coupling limit [84–86], the self-energy in QW due to the proximity effect can be obtained:

$$\hat{\Sigma}_T(\mathbf{k},\omega) = \begin{pmatrix} 0 & \hat{\Delta}^T(\mathbf{k},\omega) \\ \hat{\Delta^T}^*(\mathbf{k},\omega) & 0 \end{pmatrix}, \tag{18}$$

where

$$\hat{\Delta}^T(\mathbf{k},\omega) = \int dp_z |t_0|^2 f_{\mathbf{k}+p_z\mathbf{e_z}}^{s}(\omega). \tag{19}$$

In the weak coupling limit, the order parameters induced in QW are much smaller than Δ_0 [84–86]. Moreover, we focus on the low-frequency regime [$\omega \leqslant \Delta(\mathbf{k},\omega)$] where the main physics happens. Consequently, the frequency is much smaller than Δ_0. In this case, the frequency dependence of $\Sigma_T(\mathbf{k},\omega)$ can be neglected [58,84–86]. Therefore, by considering the small $\mathbf{k}$ in QW ($\varepsilon_{\mathbf{k}}^{s} \ll \mu_s$), one obtains (refer to Appendix A)

$$\hat{\Delta}^T(\mathbf{k},0) = \Delta_{\mathrm{SE}}^T(\mathbf{k}) i\sigma_2 = \frac{\Delta_0 |\tilde{t}|^2}{\varepsilon_{\mathbf{k}+\mathbf{q}}^{s} \varepsilon_{\mathbf{k}-\mathbf{q}}^{s} + |\Delta_0|^2 - h_B^2} i\sigma_2, \tag{20}$$

acting as the SE order parameter [$\Delta_{\mathrm{SE}}^T(\mathbf{k})$] in QW due to the proximity effect. Here, $\tilde{t}$ is the effective tunneling matrix element (given also in Appendix A).

Based on Eqs. (13) and (18), in the absence of the e-e Coulomb interaction, one can derive the Green function $G_{\mathbf{k}}(\omega)$ in QW with the proximity-induced SE order parameter included. Particularly, the anomalous Green function is

$$f_{\mathbf{k}}(\omega) = \begin{pmatrix} 0 & -\dfrac{\Delta_{\mathrm{SE}}^T(\mathbf{k})}{(\omega - E_{+\mathbf{k}}^{+})(\omega + E_{-\mathbf{k}}^{+})} \\ \dfrac{\Delta_{\mathrm{SE}}^T(\mathbf{k})}{(\omega - E_{+\mathbf{k}}^{-})(\omega + E_{-\mathbf{k}}^{-})} & 0 \end{pmatrix}, \tag{21}$$

where $E_{\nu\mathbf{k}}^{\mu} = \sqrt{\left(\frac{\xi_{\mathbf{k}+\mathbf{q}}^{c} + \xi_{\mathbf{k}-\mathbf{q}}^{c}}{2} + \mu\frac{h_{\mathbf{k}+\mathbf{q}} + h_{\mathbf{k}-\mathbf{q}}}{2}\right)^2 + |\Delta_{\mathrm{SE}}^T(\mathbf{k})|^2} + \nu\frac{\xi_{\mathbf{k}+\mathbf{q}}^{c} - \xi_{\mathbf{k}-\mathbf{q}}^{c}}{2} + \mu\nu\frac{h_{\mathbf{k}+\mathbf{q}} - h_{\mathbf{k}-\mathbf{q}}}{2}$ are the quasiparticle energy spectra ($\mu,\nu = \pm 1$) in QW. It is noted that there exist regions with $E_{\nu\mathbf{k}}^{\mu} < 0$ in the momentum space, where the quasiparticle energies are below the Fermi surface. Here, following the FFLO idea [72,73], in such regions the Cooper pairs must be broken since these quasiparticle states are perfectly blocked

by the electrons. Hence, we consider the regions with $E^{\mu}_{\nu\mathbf{k}} < 0$ are the unpairing regions where the tunneling is blocked and then the proximity-induced SE order parameter should vanish.

Consequently, the proximity-induced SE order parameter is given by

$$\Delta^{T}_{\mathrm{SE}}(\mathbf{k}) = \Delta_0 \frac{\tilde{t}^2}{\varepsilon^{s}_{\mathbf{k}+\mathbf{q}}\varepsilon^{s}_{\mathbf{k}-\mathbf{q}} + |\Delta_0|^2 - h_B^2}\hat{\delta}, \tag{22}$$

with $\delta_{\mathbf{k}} = \Pi_{\mu=\pm,\nu=\pm}\theta(E^{\mu}_{\nu\mathbf{k}})$ being the depairing operator [72]. Here, $\theta(x)$ is the step function.

From Eqs. (18) and (20), it is noted that only the SE order parameter exists. However, it is shown in the following that all four types of the order parameters can be realized in QW when the e-e Coulomb interaction is considered.

C. Self-energy due to the e-e Coulomb interaction

The self-energy in the frequency space due to the e-e Coulomb interaction reads as [80–82]

$$\hat{\Sigma}_{\mathrm{ee}}(\mathbf{k},\omega) = \frac{1}{4}\int \frac{d\mathbf{k}'}{(2\pi)^2}\frac{d\omega'}{2\pi} V_{\mathbf{k}-\mathbf{k}'}(\omega-\omega')G(\mathbf{k}',\omega'). \tag{23}$$

From Eq. (23), one observes that from the self-energy due to the e-e Coulomb interaction, the normal Green function and anomalous Green function are both renormalized. Consequently, the SOC strength, the effective mass, the zero-energy point, and the SE order parameter are renormalized. Moreover, the SO, TO, and TE order parameters can be induced due to the existence of the corresponding pairing. In this work, we focus on the renormalization-induced order parameters, and neglect the renormalization of the SOC strength, effective mass, and zero-energy point.

From Eqs. (21) and (23), the renormalization-induced order parameters can be obtained. Specifically, after the frequency integration, the renormalization-induced singlet order parameter $[\Delta_s(\mathbf{k},\omega)]$ and triplet one with zero spin projection $[\Delta_t(\mathbf{k},\omega)]$ are written as

$$\begin{aligned}\Delta_s(\mathbf{k},\omega) = &\sum_{\mu=\pm}\int \frac{d\mathbf{k}'}{32\pi^2} V^{0}_{\mathbf{k}-\mathbf{k}'}\Delta^{T}_{\mathrm{SE}}(\mathbf{k}') \\ &\times\left[\frac{1}{E^{\mu}_{+\mathbf{k}'}+E^{\mu}_{-\mathbf{k}'}}\left(\sum_{\nu=\pm}\frac{\omega^{pl}_{\mathbf{k}-\mathbf{k}'}}{E^{\mu}_{\nu\mathbf{k}'}+\omega^{pl}_{\mathbf{k}-\mathbf{k}'}-\nu\omega}-1\right)\right. \\ &+\sum_{\nu=\pm}\frac{\left|E^{\mu}_{\nu\mathbf{k}'}-\nu\omega\right|^2}{\left|E^{\mu}_{\nu\mathbf{k}'}-\nu\omega\right|^2-\left|\omega^{pl}_{\mathbf{k}-\mathbf{k}'}\right|^2}\frac{f(E^{\mu}_{\nu\mathbf{k}'})}{E^{\mu}_{+\mathbf{k}'}+E^{\mu}_{-\mathbf{k}'}} \\ &\left.+\sum_{\nu=\pm}\frac{E^{\mu}_{\nu\mathbf{k}'}-\nu\omega}{\left|E^{\mu}_{\nu\mathbf{k}'}-\nu\omega\right|^2-\left|\omega^{pl}_{\mathbf{k}-\mathbf{k}'}\right|^2}\frac{n(\omega^{pl}_{\mathbf{k}-\mathbf{k}'})\omega^{pl}_{\mathbf{k}-\mathbf{k}'}}{E^{\mu}_{+\mathbf{k}'}+E^{\mu}_{-\mathbf{k}'}}\right],\end{aligned} \tag{24}$$

$$\begin{aligned}\Delta_t(\mathbf{k},\omega) = &\sum_{\mu=\pm}\mu\int \frac{d\mathbf{k}'}{32\pi^2} V^{0}_{\mathbf{k}-\mathbf{k}'}\Delta^{T}_{\mathrm{SE}}(\mathbf{k}') \\ &\times\left[\frac{1}{E^{\mu}_{+\mathbf{k}'}+E^{\mu}_{-\mathbf{k}'}}\left(\sum_{\nu=\pm}\frac{\omega^{pl}_{\mathbf{k}-\mathbf{k}'}}{E^{\mu}_{\nu\mathbf{k}'}+\omega^{pl}_{\mathbf{k}-\mathbf{k}'}-\nu\omega}-1\right)\right. \\ &+\sum_{\nu=\pm}\frac{\left|E^{\mu}_{\nu\mathbf{k}'}-\nu\omega\right|^2}{\left|E^{\mu}_{\nu\mathbf{k}'}-\nu\omega\right|^2-\left|\omega^{pl}_{\mathbf{k}-\mathbf{k}'}\right|^2}\frac{f(E^{\mu}_{\nu\mathbf{k}'})}{E^{\mu}_{+\mathbf{k}'}+E^{\mu}_{-\mathbf{k}'}} \\ &\left.+\sum_{\nu=\pm}\frac{E^{\mu}_{\nu\mathbf{k}'}-\nu\omega}{\left|E^{\mu}_{\nu\mathbf{k}'}-\nu\omega\right|^2-\left|\omega^{pl}_{\mathbf{k}-\mathbf{k}'}\right|^2}\frac{n(\omega^{pl}_{\mathbf{k}-\mathbf{k}'})\omega^{pl}_{\mathbf{k}-\mathbf{k}'}}{E^{\mu}_{+\mathbf{k}'}+E^{\mu}_{-\mathbf{k}'}}\right],\end{aligned} \tag{25}$$

where $f(x) = [\exp(\beta x)+1]^{-1}$ is the Fermi-Dirac distribution function and $n(x) = [\exp(\beta x)-1]^{-1}$ stands for the Bose-Einstein distribution function; $\beta = 1/(k_B T)$ with k_B representing the Boltzmann constant and T being the temperature.

TABLE II. Parameters used in our calculation. Note that m_0 stands for the free-electron mass and a is the well width.

m^*_c/m_0	0.015[a]	m^*_s/m_0	3.2[b]
κ_0	16.0[a]	Δ_0 (meV)	5[b]
γ_D (eV Å^3)	79.4[c]	h_B/Δ_0	0.6[d]
a (nm)	2	T (K)	0.5
$\lvert\tilde{t}\rvert^2/\Delta_0^2$	0.5	n_0 (cm^{-2})	2.5×10^9

[a]Refs. [89,90].
[b]Ref. [91].
[c]Ref. [87].
[d]Refs. [72,73].

IV. NUMERICAL RESULTS

In this section, by calculating Eqs. (24) and (25) explicitly, we investigate the order parameters in 2DEG of the spin-orbit-coupled InSb (110) QW in proximity to s-wave superconductor in FFLO phase or with a supercurrent. All the material parameters used in our calculation are listed in Table II. As mentioned above, the frequency ω in the calculation is chosen to be smaller than Δ_0.

A. SE order parameter

In this part, we investigate the SE order parameters in QW, including the proximity-induced and renormalization-induced ones. The proximity-induced SE order parameter $\Delta^{T}_{\mathrm{SE}}(\mathbf{k})$ is obtained from Eq. (22) while the renormalization-induced one $\Delta^{R}_{\mathrm{SE}}(\mathbf{k},\omega)$ is obtained by calculating $\Delta_s(\mathbf{k},\omega)$ [Eq. (24)] explicitly:

$$\Delta^{R}_{\mathrm{SE}}(\mathbf{k},\omega) = [\Delta_s(\mathbf{k},\omega)+\Delta_s(\mathbf{k},-\omega)]/2. \tag{26}$$

1. *Momentum dependence of the proximity-induced SE order parameter: s-wave character*

We first focus on the proximity-induced SE order parameters, whose momentum dependencies at different c.m. momenta $\mathbf{q}$ are plotted in Fig. 1 at $n = 5n_0$. We find that when $q < 0.75k_F$, the proximity-induced SE order parameters $\Delta^{T}_{\mathrm{SE}}(\mathbf{k})$ show an s-wave character in the momentum space. Moreover, from Eq. (22), with $|\Delta_0| \approx \varepsilon^{s}_{16k_F}$, one finds that the strengths of the proximity-induced SE order parameters are marginally influenced when $k \ll 15k_F$ but decrease monotonically when $k > 15k_F$, as shown in Figs. 1(a) and 1(b). In addition, when $k > 15k_F$, one has $q \ll k$. Consequently, the

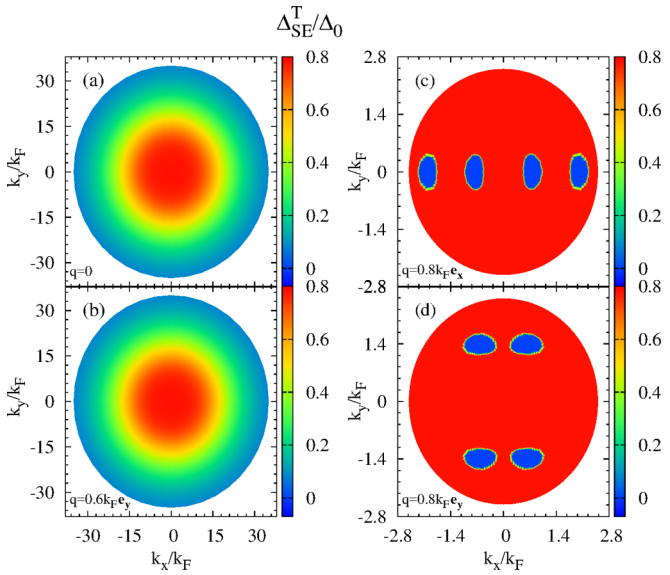

FIG. 1. Momentum dependence of the proximity-induced SE order parameter $\Delta^T_{\rm SE}(\mathbf{k})$ at (a) $\mathbf{q}=0$, (b) $\mathbf{q}=0.6k_F\mathbf{e}_x$, (c) $\mathbf{q}=0.8k_F\mathbf{e}_x$, and (d) $\mathbf{q}=0.8k_F\mathbf{e}_y$. $n=5n_0$.

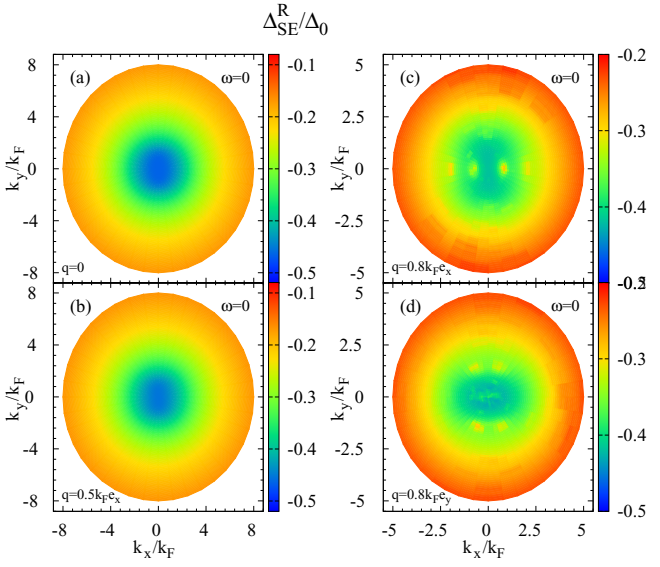

FIG. 2. Momentum dependence of the renormalization-induced SE order parameter $\Delta^R_{\rm SE}(\mathbf{k},\omega=0)$ at (a) $\mathbf{q}=0$, (b) $\mathbf{q}=0.5k_F\mathbf{e_x}$, (c) $\mathbf{q}=0.8k_F\mathbf{e_x}$, and (d) $\mathbf{q}=0.8k_F\mathbf{e_y}$. $n=5n_0$.

dependence of $\Delta^T_{\rm SE}(\mathbf{k})$ on $\mathbf{q}$ is indistinguishable, as shown by the comparison between Figs. 1(a) and 1(b).

Furthermore, it is found that when $q>0.75k_F$, there exist unpairing regions in the momentum space, where the proximity-induced SE order parameters vanish, as shown by the blue regions in Figs. 1(c) and 1(d) at $q=0.8k_F$. This is justified by the fact that the positions of the unpairing regions in the momentum space coincide with those of the regions where the depairing operator is zero (shown in Appendix B). As for the pairing region, the proximity-induced SE order parameter shows the similar behaviors to that at $q<0.75k_F$.

Consequently, the proximity-induced SE order parameter in the pairing region in QW can be considered as a constant $\Delta^T_{\rm SE}$ when $k\ll 15k_F$. It is further noted that this conclusion is consistent with the constant approximation in the previous works [58,84–86].

2. *Momentum dependence of the renormalization-induced SE order parameter: s-wave character*

We next discuss the renormalization-induced SE order parameter. The momentum dependencies of the renormalization-induced SE order parameter at different c.m. momenta are plotted in Fig. 2 when $n=5n_0$. As shown in Figs. 2(a) and 2(b), when $q<0.75k_F$, the renormalization-induced SE order parameters in the momentum space exhibit an s-wave character: $\Delta^R_{\rm SE}=C_{\rm SE}(k,\omega)$ with $C_{\rm SE}(k,\omega)$ being independent on the orientation of the momentum, similar to the proximity-induced one. Moreover, $\Delta^R_{\rm SE}$ is always in the opposite sign against the proximity-induced SE order parameter $\Delta^T_{\rm SE}$ as the renormalization from the repulsive e-e Coulomb interaction.

When $q>0.75k_F$, we find that there exist four regions in the momentum space where the renormalization-induced SE order parameters have smaller strengths than those in the region nearby [shown by the four yellow regions in the regime $k<2.1k_F$ in Figs. 2(c) or 2(d)]. The positions of these regions exactly correspond to the unpairing regions where the proximity-induced SE order parameters vanish [shown by the blue regions in Figs. 1(a) and 1(b) correspondingly]. This can be understood from the fact that the renormalization of the e-e Coulomb interaction to the SE order parameter leads to the contribution from the pairing regions to the unpairing ones.

3. *Momentum-magnitude dependence of the renormalization-induced SE order parameter*

The momentum-magnitude dependencies of the strength for the renormalization-induced SE order parameter $-\Delta^R_{\rm SE}(\mathbf{k}=k\mathbf{e_x},\omega)$ are shown in Fig. 3 at $n=5n_0$. It is first noted that at

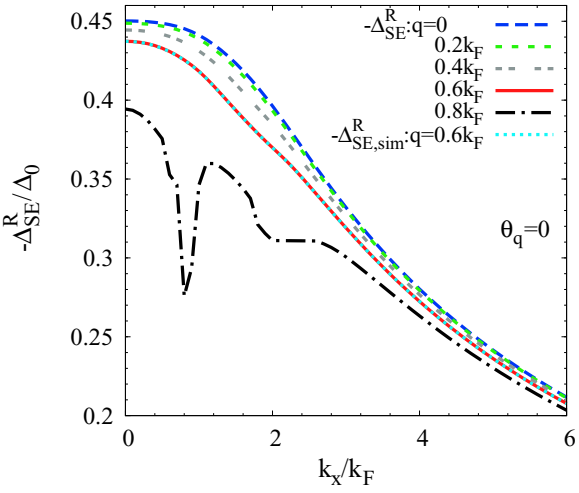

FIG. 3. Momentum-magnitude dependence of the strength for the renormalization-induced SE order parameter $|\Delta^R_{\rm SE}(\mathbf{k}=k\mathbf{e_x},\omega=0)|=-\Delta^R_{\rm SE}(\mathbf{k}=k\mathbf{e_x},\omega=0)$ at different c.m. momenta $q\mathbf{e_x}$. $n=5n_0$.

$\mathbf{q} = 0.8k_F\mathbf{e_x}$ (black chain curve), two valleys at $k \approx 0.8k_F$ and $2k_F$ are observed in the momentum-magnitude dependence, which correspond to the unpairing regions mentioned above. Whereas in the pairing regions, it is found that $-\Delta^R_{\rm SE}(\mathbf{k} = k\mathbf{e_x},\omega)$ decreases with the increase of the momentum monotonically.

The vanishing order parameter at large momentum can be understood as follows. It has been pointed out in the previous works [3,17,43,52,58] that the pairing function $f_{\mathbf{k}}(\omega)$ vanishes in QW when $\xi^c_{\mathbf{k}} \gg \Delta^T_{\rm SE}$. With the renormalization-induced order parameter $\Delta(\mathbf{k},\omega) = \int \frac{d\omega' d\mathbf{k}'}{4(2\pi)^3} \frac{V^0_{\mathbf{k}-\mathbf{k}'} f_{\mathbf{k}'}(\omega')}{\epsilon(\omega-\omega')}$, one has $\Delta(\mathbf{k},\omega) \propto \int d\omega' \frac{f_{\mathbf{k}}(\omega')}{\epsilon(\omega-\omega')}$ since the Coulomb interaction $V^0_{\mathbf{k}-\mathbf{k}'}$ is very strong at $\mathbf{k}' = \mathbf{k}$ and can be approximated by a delta function: $\delta(\mathbf{k}'-\mathbf{k})$ in the analytic analysis. Therefore, the order parameter vanishes at large momentum when $\xi^c_{\mathbf{k}} \gg \Delta^T_{\rm SE}$ due to the vanishing pairing function.

This vanishing of the SE order parameter can also be understood from Eq. (24). Specifically, after some simplifications at low temperature (refer to Appendix C), the renormalization-induced SE order parameter can be approximately written as

$$-\Delta^R_{\rm SE}(\mathbf{k},\omega) \approx \int \frac{d\mathbf{k}'}{16\pi^2} \frac{V^0_{\mathbf{k}-\mathbf{k}'}\Delta^T_{\rm SE}}{F_{k'}} \times \left[1 - \frac{\omega^{pl}_{\mathbf{k}-\mathbf{k}'}}{F_{k'}}\left(1+\frac{\omega^2}{F^2_{k'}}\right) - \frac{\xi^c_{\mathbf{k}'}\varepsilon^c_{\mathbf{q}}}{F^2_{k'}}\right], \quad (27)$$

where $F_{k'} = \sqrt{|\xi^c_{\mathbf{k}'}|^2 + |\Delta^T_{\rm SE}|^2}$.

Then, the momentum-magnitude dependence of the renormalization-induced SE order parameter can be analyzed. Specifically, by approximately taking the Coulomb interaction $V^0_{\mathbf{k}-\mathbf{k}'}$ in Eq. (27) as a delta function $\delta(\mathbf{k}-\mathbf{k}')$ for the analytic analysis, one has $-\Delta^R_{\rm SE}(\mathbf{k},\omega) \propto 1/\sqrt{|\xi^c_{\mathbf{k}}|^2 + |\Delta^T_{\rm SE}|^2}$. Then, at $\xi^c_k \ll \Delta^T_{\rm SE} \approx \xi^c_{3k_F}$ ($\xi^c_k \gg \Delta^T_{\rm SE}$), $-\Delta^R_{\rm SE}(\mathbf{k},\omega)$ is marginally changed (decreases) with the increase of the momentum, as shown in Fig. 3. This conclusion is in agreement with the one from the analysis of the pairing function proposed above.

Furthermore, from Eq. (27) the c.m. momentum dependence of $\Delta^R_{\rm SE}$ can also be understood. In the integral of Eq. (27), the third term makes the important contribution only when $|\xi^c_{k'}| \sim F_{k'}$ where $\xi^c_{k'} > \xi^c_{3k_F}$. Hence, the increase of q leads to the decrease of $-\Delta^R_{\rm SE}$, as shown in Fig. 3.

B. SO order parameter

In this part, we investigate the induced SO order parameter in QW by calculating $\Delta_s(\mathbf{k},\omega)$ [Eq. (24)] explicitly. Then, the induced SO order parameter is obtained:

$$\Delta_{\rm SO}(\mathbf{k},\omega) = [\Delta_s(\mathbf{k},\omega) - \Delta_s(\mathbf{k},-\omega)]/2. \quad (28)$$

For the analytic analysis, similar to the study on the renormalization-induced SE order parameters in Sec. IV A, by taking some simplifications (refer to Appendix C), the SO order parameter can be approximately written as

$$\Delta_{\rm SO}(\mathbf{k},\omega) = \Delta^K_{\rm SO}(\mathbf{k},\omega) + \Delta^S_{\rm SO}(\mathbf{k},\omega), \quad (29)$$

with

$$\Delta^K_{\rm SO}(\mathbf{k},\omega) = -\omega \int \frac{d\mathbf{k}'}{16\pi^2} V^0_{\mathbf{k}-\mathbf{k}'}\Delta^T_{\rm SE}\frac{\omega^{pl}_{\mathbf{k}-\mathbf{k}'}}{F^4_{k'}}\frac{\mathbf{k}'\cdot\mathbf{q}}{m^*_c}, \quad (30)$$

$$\Delta^S_{\rm SO}(\mathbf{k},\omega) = \omega \int \frac{d\mathbf{k}'}{16\pi^2} V^0_{\mathbf{k}-\mathbf{k}'}\Delta^T_{\rm SE}\frac{\omega^{pl}_{\mathbf{k}-\mathbf{k}'}}{F^4_{k'}}\frac{2h_{\mathbf{q}}h_{\mathbf{k}'}\xi^c_{\mathbf{k}'}}{F^2_{k'}} = \omega \int \frac{d\mathbf{k}'}{16\pi^2} V^0_{\mathbf{k}-\mathbf{k}'}\Delta^T_{\rm SE}\frac{\omega^{pl}_{\mathbf{k}-\mathbf{k}'}}{F^4_{k'}}\Gamma_{k'}\frac{k'_x q_x}{m^*_c}. \quad (31)$$

Here, $\Gamma_{k'} = |\gamma_D\langle k_z^2\rangle|^2\xi_{k'}m^*_c/F^2_{k'}$. The first term $\Delta^K_{\rm SO}(\mathbf{k},\omega)$ in Eq. (29) comes from the broken translational symmetry by the c.m. momentum of Cooper pair ($q \neq 0$) in the system, whereas the second one $\Delta^S_{\rm SO}(\mathbf{k},\omega)$ is induced due to the coupling between the c.m. momentum and SOC from the high-order expansion. Hence, $\Delta^K_{\rm SO}(\mathbf{k},\omega)$ makes the leading contribution in Eq. (29). Additionally, it is noted that $\Delta_{\rm SO}(\mathbf{k},\omega)$ arises from the retardation effect in the effective attractive potential $V^{\rm at}_{\mathbf{k}}(\omega)$, in accord with the previous works [12–17]. In the following, we show that from Eq. (29), the momentum and dependence of the SO order parameter can be analyzed, in good agreement with the full numerical results.

1. *Momentum dependence of the SO order parameter: p-wave character*

In this section, we focus on the momentum dependencies of the SO order parameter $\Delta_{\rm SO}(\mathbf{k},\omega = E_F)$ at different c.m. momenta $\mathbf{q}$. The full numerical results are plotted in Fig. 4 at $n = 5n_0$. As seen from the figure, it is found that the SO order parameter in the momentum space exhibits a p-wave character: $\Delta_{\rm SO} = C_{\rm SO}(k,\omega)\mathbf{k}\cdot\mathbf{q}$ with $C_{\rm SO}(k,\omega)$ being independent on the orientation of the momentum (demonstrated in Appendix D). This can be understood as follows. With the Fermi-Dirac statistics for the SO order parameter, one finds $\Delta_{\rm SO}(\mathbf{k},\omega) = -\Delta_{\rm SO}(-\mathbf{k},\omega)$. In addition, the system in QW

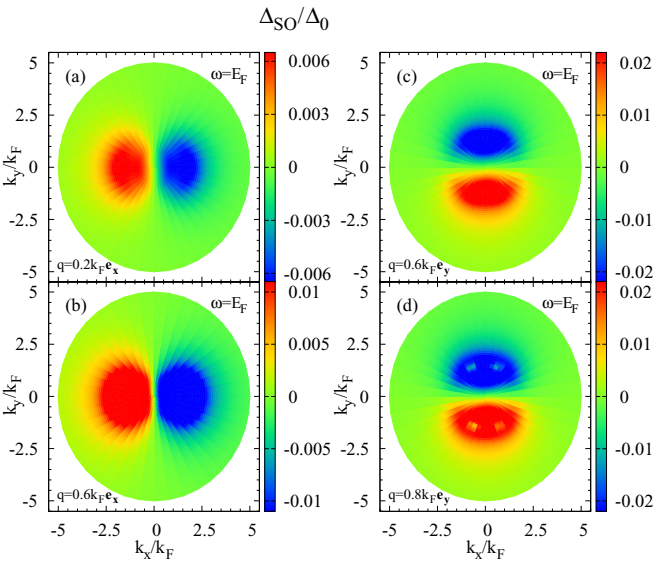

FIG. 4. Momentum dependence of the SO order parameter $\Delta_{\rm SO}(\mathbf{k},\omega = E_F)$ at (a) $\mathbf{q} = 0.2k_F\mathbf{e_x}$, (b) $\mathbf{q} = 0.6k_F\mathbf{e_x}$, (c) $\mathbf{q} = 0.6k_F\mathbf{e_y}$, and (d) $\mathbf{q} = 0.8k_F\mathbf{e_y}$. $n = 5n_0$.

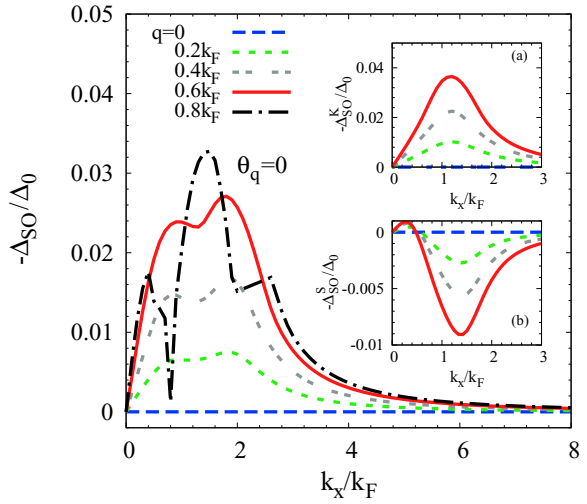

FIG. 5. Momentum-magnitude dependence of the strength for the SO order parameter $|\Delta_{\rm SO}(\mathbf{k}=k\mathbf{e}_{\mathbf{x}},\omega=E_F)|=-\Delta_{\rm SO}(\mathbf{k}=k\mathbf{e}_{\mathbf{x}},\omega=E_F)$ at different c.m. momenta $q\mathbf{e}_{\mathbf{x}}$. The inset (a) [(b)] shows the calculated results for $-\Delta^K_{\rm SO}(\mathbf{k}=k\mathbf{e}_{\mathbf{x}},\omega=E_F)$ [$-\Delta^S_{\rm SO}(\mathbf{k}=k\mathbf{e}_{\mathbf{x}},\omega=E_F)$] from Eq. (30) [Eq. (31)]. $n=5n_0$.

has the spatial-rotational symmetry around the $\mathbf{q}$ axis in the momentum space, and then one has $\Delta_{\rm SO}(\mathbf{k},\omega)=\Delta_{\rm SO}(-\mathbf{k},\omega)$ when $\mathbf{k}\perp\mathbf{q}$. Hence, the vanishing $\Delta_{\rm SO}(\mathbf{k},\omega)$ at $\mathbf{k}\perp\mathbf{q}$ is immediately obtained and the SO order parameter exhibits as $\Delta_{\rm SO}(\mathbf{k},\omega)\propto\mathbf{k}\cdot\mathbf{q}$ at small q.

From Eq. (29), one can obtain the same conclusion. Specifically, by approximately taking the Coulomb interaction $V^0_{\mathbf{k}-\mathbf{k}'}\omega^{pl}_{\mathbf{k}-\mathbf{k}'}\propto 1/\sqrt{|\mathbf{k}-\mathbf{k}'|}$ as a delta function, one has $\Delta_{\rm SO}(\mathbf{k},\omega)\propto\mathbf{k}\cdot\mathbf{q}$. Additionally, it is noted that small strengths of the SO order parameter are observed in the unpairing regions at $q=0.8k_F$ [shown by the four green regions in Fig. 4(d)] due to the renormalization of the e-e Coulomb interaction, similar to the renormalization-induced SE order parameter.

2. *Momentum-magnitude dependence of the SO order parameter*

The momentum-magnitude dependencies of the SO order parameter are shown in Fig. 5 at different c.m. momenta $q\mathbf{e}_{\mathbf{x}}$. As seen from the figure, when $q=0$, with the translational symmetry, the SO order parameter $\Delta_{\rm SO}=0$ (blue dashed curve). When $q=0.8k_F$ (black chain curve), two valleys are observed at $0.8k_F$ and $2k_F$, exactly corresponding to the unpairing regions, similar to the results of the renormalization-induced SE order parameter. When $0<q<0.8k_F$, it is shown that the strength of the SO order parameter exhibits double-peak behavior with the increase of the momentum.

Specifically, one finds that $\Delta_{\rm SO}(\mathbf{k}=0,\omega)=0$ due to the odd parity and $|\Delta_{\rm SO}(\mathbf{k},\omega)|\propto\mathbf{k}\cdot\mathbf{q}$ increases with increasing momentum at small k. As for the large momentum, due to the vanishing pairing function at $\xi^c_k\gg\Delta^T_{\rm SE}$ mentioned in Sec. IV A, one has $\Delta_{\rm SO}(\mathbf{k},\omega)=0$. Hence, peaks of the strength for the SO order parameter in-between are expected. Similarly, peaks for $|\Delta^K_{\rm SO}(\mathbf{k},\omega)|$ and $|\Delta^S_{\rm SO}(\mathbf{k},\omega)|$ are also expected, as shown in the insets (a) and (b) in Fig. 5 where we plot $-\Delta^K_{\rm SO}(\mathbf{k},\omega)=|\Delta^K_{\rm SO}(\mathbf{k},\omega)|$ and $-\Delta^S_{\rm SO}(\mathbf{k},\omega)=-|\Delta^S_{\rm SO}(\mathbf{k},\omega)|$ at $\mathbf{q}=q\mathbf{e}_{\mathbf{x}}$, respectively. Hence, with the peak of $-\Delta^K_{\rm SO}$ and the valley of $-\Delta^S_{\rm SO}$ shown in the insets (a) and (b) of Fig. 5, respectively, the strength of the SO order parameter $-\Delta_{\rm SO}(\mathbf{k},\omega)=-\Delta^K_{\rm SO}(\mathbf{k},\omega)-\Delta^S_{\rm SO}(\mathbf{k},\omega)$ exhibits the double-peak structure in the momentum-magnitude dependence. Particularly, it is found that at the case $\mathbf{q}=q\mathbf{e}_{\mathbf{y}}$, with $\Delta^S_{\rm SO}\approx 0$, the strength of the SO order parameter $-\Delta_{\rm SO}(\mathbf{k},\omega)=-\Delta^K_{\rm SO}(\mathbf{k},\omega)$ shows one-peak structure (not shown in the figure).

From Eq. (30) [Eq. (31)], the peak positions for $|\Delta^K_{\rm SO}(\mathbf{k},\omega)|$ and $|\Delta^S_{\rm SO}(\mathbf{k},\omega)|$ at $q\mathbf{e}_{\mathbf{x}}$ can be determined explicitly. Specifically, by considering the Coulomb interaction $V^0_{\mathbf{k}-\mathbf{k}'}\omega^{pl}_{\mathbf{k}-\mathbf{k}'}$ as a delta function for the analytic analysis, one has $|\Delta^K_{\rm SO}|\propto\mathbf{k}\cdot\mathbf{q}/(|\xi^c_{\mathbf{k}}|^2+|\Delta^T_{\rm SE}|^2)^2$ [$|\Delta^S_{\rm SO}|\propto\mathbf{k}\cdot\mathbf{q}\varepsilon^c_k/(|\xi^c_{\mathbf{k}}|^2+|\Delta^T_{\rm SE}|^2)^3$], exhibiting one-peak behavior in the momentum-magnitude dependence. Then, by calculating the maxima of $\mathbf{k}\cdot\mathbf{q}/(|\xi^c_{\mathbf{k}}|^2+|\Delta^T_{\rm SE}|^2)^2$ and $\mathbf{k}\cdot\mathbf{q}\varepsilon^c_k/(|\xi^c_{\mathbf{k}}|^2+|\Delta^T_{\rm SE}|^2)^3$, the peak positions for $|\Delta^K_{\rm SO}|$ and $|\Delta^S_{\rm SO}|$ can be determined at $k^p_K\approx\sqrt{3+\sqrt{9+7(1+|\Delta^T_{\rm SE}|^2E_F^{-2})}}k_F/\sqrt{7}=1.15k_F$ and $k^p_S\approx\sqrt{1+\sqrt{1+3(1+|\Delta^T_{\rm SE}|^2E_F^{-2})}}k_F/\sqrt{3}=1.26k_F$, respectively, very close to those from the numerical calculation shown in the insets (a) and (b) of Fig. 5. Then, the valley position between the two peaks in the momentum-magnitude dependence for $-\Delta_{\rm SO}(\mathbf{k},\omega)$ can be determined at $k^p_S\approx 1.26k_F$, close to the one from full numerical results shown in Fig. 5.

Furthermore, due to the broken translational symmetry by the c.m. momentum $\mathbf{q}$, the strength of the induced SO order parameter increases with the increase of q as shown in Fig. 5, in accord with Eq. (29).

C. TE order parameter

In this section, we focus on the TE order parameters in QW by numerically calculating $\Delta_t(\mathbf{k},\omega)$ [Eq. (25)]. The induced TE order parameter is obtained:

$$\Delta_{\rm TE}(\mathbf{k},\omega)=[\Delta_t(\mathbf{k},\omega)+\Delta_t(\mathbf{k},-\omega)]/2. \tag{32}$$

For the analytic analysis, similar to the study on the SE order parameter, by taking some simplifications (refer to Appendix C), the induced TE order parameter can be approximately written as

$$\Delta_{\rm TE}(\mathbf{k},\omega)=\int\frac{d\mathbf{k}'}{16\pi^2}\frac{V^0_{\mathbf{k}-\mathbf{k}'}\Delta^T_{\rm SE}}{F^3_{k'}}h_{\mathbf{k}'}\xi^c_{\mathbf{k}'}\times\left[1-\frac{2\omega^{pl}_{\mathbf{k}-\mathbf{k}'}}{F_{k'}}\left(1+\frac{\omega^2}{F^2_{\mathbf{k}'}}\right)-\frac{3\xi^c_{\mathbf{k}'}\varepsilon^c_{\mathbf{q}}}{F^2_{k'}}\right]. \tag{33}$$

It is noted that the TE order parameter is induced due to the broken spin-rotational symmetry by the SOC ($h_{\mathbf{k}}\neq 0$). In the following, we show that from Eq. (33), the momentum dependence of the TE order parameter can be analyzed in accord with the numerical results well.

1. *Momentum dependence of the TE order parameter: p-wave character*

In this section, we show the momentum dependencies of the TE order parameter $\Delta_{\rm TE}(\mathbf{k},\omega=0)$ at different c.m. momenta

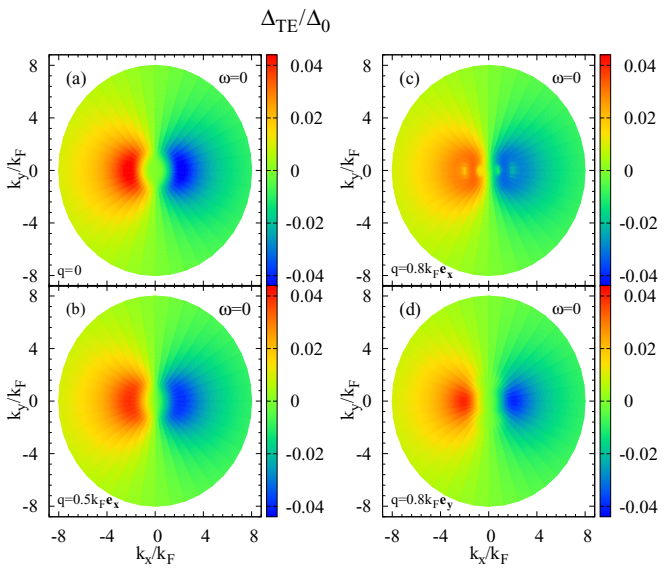

FIG. 6. Momentum dependence of the TE order parameter $\Delta_{\rm TE}(\mathbf{k},\omega=0)$ at (a) $\mathbf{q}=0$, (b) $\mathbf{q}=0.5k_F\mathbf{e}_\mathbf{x}$, (c) $\mathbf{q}=0.8k_F\mathbf{e}_\mathbf{x}$, and (d) $\mathbf{q}=0.8k_F\mathbf{e}_\mathbf{y}$. $n=5n_0$.

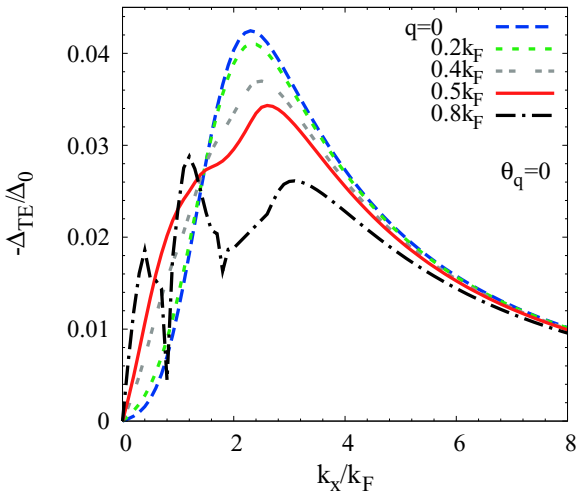

FIG. 7. Momentum-magnitude dependence of the strength for the TE order parameter $|\Delta_{\rm TE}(\mathbf{k}=k\mathbf{e}_\mathbf{x},\omega=0)|=-\Delta_{\rm TE}(\mathbf{k}=k\mathbf{e}_\mathbf{x},\omega=0)$ at different c.m. momenta $q\mathbf{e}_\mathbf{x}$. $n=5n_0$.

$\mathbf{q}$. The full numerical results are plotted in Fig. 6 at $n=5n_0$. As seen from the figure, the TE order parameter exhibits a p-wave character in the momentum space: $\Delta_{\rm TE}=C_{\rm TE}(k,\omega)\mathbf{k}\cdot\mathbf{e}_\mathbf{x}$ with $C_{\rm TE}(k,\omega)$ being independent on the orientation of the momentum (demonstrated in Appendix D). Differing from the p-wave character of the SO order parameter which shows anisotropy with respect to the direction of $\mathbf{q}$ (as shown in Fig. 4) [$\Delta_{\rm SO}(\mathbf{k},\omega)=C_{\rm SO}(k,\omega)\mathbf{k}\cdot\mathbf{q}$], the p-wave character of the TE order parameter is independent on the direction of $\mathbf{q}$. This is because the TE order parameter is induced due to the spin-rotational asymmetry by the SOC. This can also be understood from Eq. (33) by approximately taking the Coulomb interaction $V^0_{\mathbf{k}-\mathbf{k}'}$ as a delta function: one has $\Delta_{\rm TE}(\mathbf{k},\omega)\propto h_\mathbf{k}\propto k_x$.

Moreover, it is noted in Fig. 6(c) that small strengths of the TE order parameter are observed in the unpairing regions at $q=0.8k_F$ (shown by the four green regions with the smaller order parameters than the region nearby) due to the renormalization of the e-e Coulomb interaction, similar to the renormalization-induced SE and SO ones.

2. *Momentum-magnitude dependence of the TE order parameter*

The momentum-magnitude dependencies of the TE order parameter $|\Delta_{\rm TE}(\mathbf{k}=k\mathbf{e}_\mathbf{x},\omega)|$ are shown in Fig. 7 at different c.m. momenta $q\mathbf{e}_\mathbf{x}$ when $n=5n_0$. As seen from the figure, when $q=0.8k_F$, two valleys are observed at $0.8k_F$ and $2k_F$ in the momentum-magnitude dependence (black chain curve), corresponding to the unpairing regions mentioned above. When $q<0.8k_F$, with the increase of the momentum, $|\Delta_{\rm TE}(\mathbf{k}=k\mathbf{e}_\mathbf{x},\omega)|$ first increases when $k<2.3k_F$ then decreases after $k>2.3k_F$, leading to a peak around $k\approx 2.3k_F$.

The peak behavior can be understood as follows. Since the TE order parameter is induced by the SOC, with the increase of the momentum at small (large) momentum, the TE order parameter is enhanced (suppressed) by the enhanced SOC (suppressed pairing function mentioned in Sec. IV A), leading to the peak in the momentum-magnitude dependence. This conclusion is in good agreement with Eq. (33), from which one finds that $|\Delta_{\rm TE}(\mathbf{k},\omega)|\propto|h_\mathbf{k}\xi^c_\mathbf{k}|/|\sqrt{\xi_k^2+|\Delta^T_{\rm SE}|^2}|^3$ by approximately taking the Coulomb interaction $V^0_{\mathbf{k}-\mathbf{k}'}$ as a delta function. Then, through the similar analysis of the momentum-magnitude peak for the strength of the SO order parameter in Sec. IV B, the equation of the momentum-magnitude peak position $k^p_{\rm TE}$ for the strength of the TE order parameter can be obtained:

$$3\left(\left|\frac{k^p_{\rm TE}}{k_F}\right|^2-1\right)^2\left(\left|\frac{k^p_{\rm TE}}{k_F}\right|^2+1\right)=2\left|\frac{\Delta^T_{\rm SE}}{E_F}\right|^2\left(3\left|\frac{k^p_{\rm TE}}{k_F}\right|^2-1\right). \tag{34}$$

From Eq. (34), one has $k^p_{\rm TE}\approx 2.1k_F$, very close to the position from the full numerical calculation shown in Fig. 7.

Moreover, the c.m. momentum dependence of the TE order parameter can also be analyzed. Specifically, from Eq. (33), by approximately taking the Coulomb interaction $V^0_{\mathbf{k}-\mathbf{k}'}$ as a delta function, one finds that with the increase of q, $|\Delta_{\rm TE}(\mathbf{k},\omega)|$ increases when $k<k_F$ and decreases when $k>k_F$, in accord with the numerical results in Fig. 7.

D. TO order parameter

In this section, we investigate the TO order parameters in QW through the numerical calculation of $\Delta_t(\mathbf{k},\omega)$ [Eq. (25)]. The induced TO order parameter is obtained:

$$\Delta_{\rm TO}(\mathbf{k},\omega)=[\Delta_t(\mathbf{k},\omega)-\Delta_t(\mathbf{k},-\omega)]/2. \tag{35}$$

As for the analytic analysis, similar to the study on the TE order parameter in Sec. IV C, by taking some simplifications (refer to Appendix C), the TO order parameter can approximately be

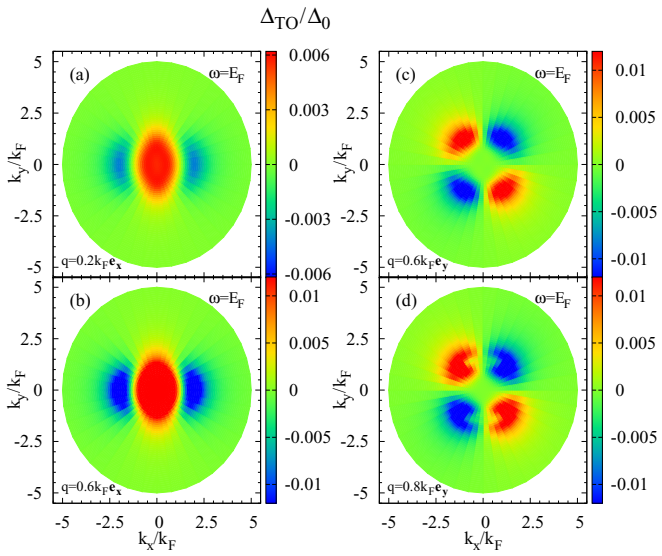

FIG. 8. Momentum dependence of the TO order parameter $\Delta_{\rm TO}(\mathbf{k},\omega=E_F)$ at (a) $\mathbf{q}=0.2k_F\mathbf{e_x}$, (b) $\mathbf{q}=0.6k_F\mathbf{e_x}$, (c) $\mathbf{q}=0.6k_F\mathbf{e_y}$, and (d) $\mathbf{q}=0.8k_F\mathbf{e_y}$. $n=5n_0$.

written as

$$\Delta_{\rm TO}(\mathbf{k},\omega) = -\omega\int\frac{d\mathbf{k}'}{16\pi^2}\frac{\omega^{pl}_{\mathbf{k}-\mathbf{k}'}V^0_{\mathbf{k}-\mathbf{k}'}\Delta^T_{\rm SE}}{F^4_{k'}} \times\left(h_{\mathbf{q}}-\frac{\mathbf{k}'\cdot\mathbf{q}}{m^*_c}\frac{h_{\mathbf{k}'}\xi^c_{\mathbf{k}'}}{F^2_{k'}}\right) \approx \omega\gamma_D\langle k_z^2\rangle\int\frac{d\mathbf{k}'}{16\pi^2}\frac{\omega^{pl}_{\mathbf{k}-\mathbf{k}'}V^0_{\mathbf{k}-\mathbf{k}'}\Delta^T_{\rm SE}}{F^4_{k'}} \times\left(q_x-\frac{\mathbf{k}'\cdot\mathbf{q}}{m^*_c}\frac{k'_x\xi^c_{\mathbf{k}'}}{F^2_{k'}}\right). \quad (36)$$

It is noted that the TO order parameter is induced due to the spin-rotational asymmetry by the SOC ($h_{\mathbf{k}}\neq 0$) and the translational asymmetry ($q\neq 0$). Additionally, the TO order parameter comes from the retardation effect in the effective attractive potential $V^{\rm at}_{\mathbf{k}}(\omega)$, in accord with the previous works [4–8,17]. In the following, we show that from Eq. (36), the momentum dependence of the TO order parameter can be analyzed, in good agreement with the numerical results.

1. *Momentum dependence of the TO order parameter: d_{x^2}- and d_{xy}-wave characters*

In this section, we focus on the momentum dependencies of the TO order parameter at different c.m. momenta $\mathbf{q}$, which are plotted in Fig. 8 at $n=5n_0$. We find that the TO order parameter shows a d-wave character in the momentum space: $\Delta_{\rm TO}(\mathbf{k},\omega)=C^0_{\rm TO}(k,\omega)\mathbf{q}\cdot\mathbf{e_x}-C^1_{\rm TO}(k,\omega)(\mathbf{k}\cdot\mathbf{e_x})(\mathbf{k}\cdot\mathbf{q})$ with $C^0_{\rm TO}(k,\omega)$ and $C^1_{\rm TO}(k,\omega)$ being independent on the orientation of the momentum (demonstrated in Appendix D). Particularly, at $\mathbf{q}=q\mathbf{e_x}$ ($\mathbf{q}=q\mathbf{e_y}$), the TO order parameters exhibit a d_{x^2}-wave (d_{xy}-wave) character: $\Delta_{\rm TO}(\mathbf{k},\omega)=(C^0_{\rm TO}-C^1_{\rm TO}k_x^2)q$ [$\Delta_{\rm TO}(\mathbf{k},\omega)=-C^1_{\rm TO}k_xk_yq$], as shown in Fig. 8(b) [8(c)]. This is due to the unique SOC in InSb (110) QW. Specifically, by approximately taking the Coulomb interaction $V^0_{\mathbf{k}-\mathbf{k}'}\omega^{pl}_{\mathbf{k}-\mathbf{k}'}$ as a delta function in Eq. (36), one has $\Delta_{\rm TO}(\mathbf{k},\omega)\propto[q_x-k_x(\mathbf{k}\cdot\mathbf{q})\xi^c_k/(m^*_cF^2_k)]$, in good agreement with the full numerical results.

Additionally, it is noted that small strengths of the TO order parameter are observed in the unpairing regions at $q=0.8k_F$ [four concave parts shown in Fig. 8(d)] due to the renormalization of the e-e Coulomb interaction, similar to the renormalization-induced SE, SO, and TE ones.

2. *Momentum-magnitude dependence of the TO order parameter*

The momentum-magnitude dependencies of the TO order parameter are shown in Fig. 9 at different c.m. momenta $\mathbf{q}$ when $n=5n_0$. We first discuss the case at $\mathbf{q}=q\mathbf{e_x}$. It is noted that at $q=0.8k_F$, a valley and a peak of the TO order parameter in the momentum-magnitude dependence are observed at $0.8k_F$ and $2k_F$ [black chain curve in Fig. 9(a)], respectively, which exactly correspond to the unpairing regions mentioned above, similar to the previous results of SE, SO, and TE ones. In addition, as shown in Fig. 9(a) at $\mathbf{q}=q\mathbf{e_x}$, when $q<0.8k_F$, with the increase of the momentum, the TO order

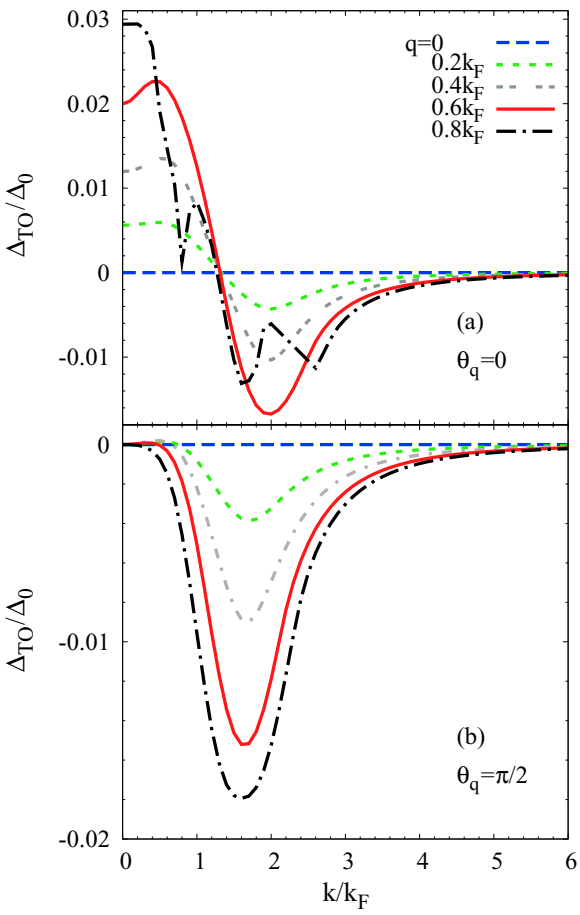

FIG. 9. Momentum-magnitude dependence of the TO order parameter for (a) $\Delta_{\rm TO}(\mathbf{k}=k\mathbf{e_x},\omega=E_F)$ at $\mathbf{q}=q\mathbf{e_x}$ and (b) $\Delta_{\rm TO}(\mathbf{k}=k\mathbf{e_c},\omega=E_F)$ at $\mathbf{q}=q\mathbf{e_y}$. $n=5n_0$. $\mathbf{e_c}$ is the unit vector along the $\mathbf{e_x}+\mathbf{e_y}$ direction.

parameter $\Delta_{\rm TO}(\mathbf{k}=k\mathbf{e}_\mathbf{x},\omega)$, possessing the same sign with Δ_0 at $k=0$, first increases when $k<0.5k_F$ then decreases when $0.5<k_F<2k_F$, leading to a peak around $0.5k_F$. Moreover, when $0.5<k_F<2k_F$, it is noted that $\Delta_{\rm TO}(\mathbf{k}=k\mathbf{e}_\mathbf{x},\omega)$ has a sign change at $1.4k_F$, and shows opposite sign against Δ_0 when $k>1.4k_F$. With further increasing the momentum when $k>2k_F$, the TO order parameter tends to zero, leading to a valley around $2k_F$.

This momentum-magnitude dependence of the TO order parameter is more complex than the previous SE, SO, and TE ones. Nevertheless, we show that from Eq. (36), this dependence can be well understood. Specifically, by approximately taking the Coulomb interaction $V^0_{\mathbf{k}-\mathbf{k}'}\omega^{pl}_{\mathbf{k}-\mathbf{k}'}$ as a delta function, at $\mathbf{q}=q\mathbf{e}_\mathbf{x}$, one has

$$\Delta_{\rm TO}(\mathbf{k}=k\mathbf{e}_\mathbf{x},\omega=E_F)\propto\left[1+\varepsilon^c_k\left(E_F-\varepsilon^c_k\right)/F^2_k\right]/F^4_k, \tag{37}$$

with same sign to Δ_0 at $k=0$. When $k\ll 3k_F$ with $F_k\approx\Delta^T_{\rm SE}$, from Eq. (37), it is found that the increase of the momentum at $k<0.5k_F$ ($k>0.5k_F$) leads to the increase (decrease) of $\Delta_{\rm TO}(\mathbf{k}=k\mathbf{e}_\mathbf{x},\omega)$ and the peak around $0.5k_F$. Moreover, when $0.5k_F<k\ll 3k_F$, it is noted that the TO order parameter $\Delta_{\rm TO}(\mathbf{k}=k\mathbf{e}_\mathbf{x},\omega)$ has a sign change at $k=(1+|\Delta^T_{\rm SE}/E_F|^2)^{1/4}k_F\approx 1.42k_F$ where one has $\Delta_{\rm TO}(\mathbf{k}=k\mathbf{e}_\mathbf{x},\omega=E_F)=0$ in Eq. (37), and then $\Delta_{\rm TO}(\mathbf{k}=k\mathbf{e}_\mathbf{x},\omega)$ is in opposite sign against Δ_0 at $k>1.42k_F$. With further increasing the momentum, the suppression of the pairing function, i.e., the increase of F_k, leads to the suppression on the TO order parameter, and hence $\Delta_{\rm TO}(\mathbf{k}=k\mathbf{e}_\mathbf{x},\omega)$ tends to zero, leading to the valley observed. The valley position can be determined by calculating the minimum of $\Delta_{\rm TO}(\mathbf{k}=k\mathbf{e}_\mathbf{x},\omega)$ at $k^v_{\rm TO}\approx(3+|\Delta^T_{\rm SE}/E_F|^2+|\Delta^T_{\rm SE}/E_F|\sqrt{3+|\Delta^T_{\rm SE}/E_F|^2})k_F/3=1.9k_F$, again very close to the one from the full numerical results in Fig. 9(a).

For the case at $\mathbf{q}=q\mathbf{e}_\mathbf{y}$, it is found that $\Delta_{\rm TO}(\mathbf{k}=k\mathbf{e}_\mathbf{c},\omega)\propto\varepsilon^c_k(E_F-\varepsilon^c_k)/F^6_k$ ($\mathbf{e}_\mathbf{c}$ is defined as the unit vector along $\mathbf{e}_\mathbf{x}+\mathbf{e}_\mathbf{y}$ direction), similar to Eq. (37) at $\mathbf{q}=q\mathbf{e}_\mathbf{x}$. Consequently, by using the similar analysis, one may understand the behavior in Fig. 9(b) well.

Furthermore, with the translational asymmetry broken by the c.m. momentum $\mathbf{q}$, it is found that the strengths of the induced TO order parameters $|\Delta_{\rm TO}(\mathbf{k},\omega)|$ increase with the increase of the c.m. momentum from Eq. (36), as shown in Fig. 9.

E. Separation of the order parameters containing all four types

Finally, we compare the four types of the order parameters in QW and propose a tentative way to distinguish these order parameters in the experiment. Specifically, through the study of the density dependencies of the four types of the order parameters in detail (refer to Appendix E), it is found that at small density, due to the suppressed attractive potential $V^{\rm at}_\mathbf{k}$, the renormalization-induced SE order parameter $\Delta^R_{\rm SE}$, with its sign being opposite against the proximity-induced one $\Delta^T_{\rm SE}$, is markedly enhanced. Then, the SE order parameter $\Delta_{\rm SE}=\Delta^T_{\rm SE}+\Delta^R_{\rm SE}$ is efficiently suppressed at small density, similar to the previous work [58]. In this case, the SO (induced by c.m. momentum of Cooper pair), TE (induced by the SOC), and TO (induced by the SOC and c.m. momentum) order parameters are dominant.

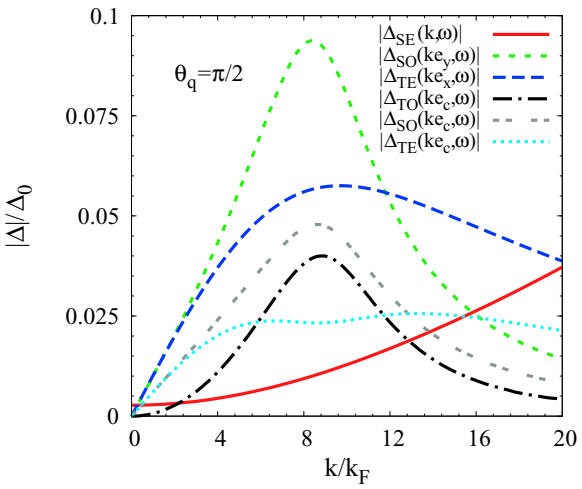

FIG. 10. Momentum-magnitude dependence of the order parameter of each symmetry containing all four types at $\mathbf{q}=10k_F\mathbf{e}_\mathbf{y}$. It is also found that $\Delta_{\rm SO}(\mathbf{k}=k\mathbf{e}_\mathbf{x},\omega)=\Delta_{\rm TE}(\mathbf{k}=k\mathbf{e}_\mathbf{y},\omega)=\Delta_{\rm TO}(\mathbf{k}=k\mathbf{e}_\mathbf{x},\omega)=\Delta_{\rm TO}(\mathbf{k}=k\mathbf{e}_\mathbf{y},\omega)=0$ from the full numerical results at $\mathbf{q}=10k_F\mathbf{e}_\mathbf{y}$ (not shown in the figure). $n=0.15n_0$ and $\omega=15E_F\ll\Delta^T_{\rm SE}$.

Furthermore, as summarized in Table I, the SO (TE) order parameter in the momentum space exhibits a p-wave character while the TO one exhibits a d-wave character. Particularly, when $\mathbf{q}=q\mathbf{e}_\mathbf{y}$, from Table I, one has $\Delta_{\rm SO}(\mathbf{k},\omega)=C_{\rm SO}(k,\omega)qk_y$, $\Delta_{\rm TE}(\mathbf{k},\omega)=C_{\rm TE}(k,\omega)k_x$, and $\Delta_{\rm TO}(\mathbf{k},\omega)=-C^1_{\rm TO}(k,\omega)k_xk_y$. In this case, with the suppressed SE order parameter at small density, along the $\mathbf{e}_\mathbf{y}$ ($\mathbf{e}_\mathbf{x}$) direction in the momentum space with $\Delta_{\rm TE}=\Delta_{\rm TO}=0$ ($\Delta_{\rm SO}=\Delta_{\rm TO}=0$), the SO (TE) order parameter can be detected solely and then $C_{\rm SO}(k,\omega)$ [$C_{\rm TE}(k,\omega)$] can be determined explicitly.

The full numerical results of the four types of the order parameters at small density $n=0.15n_0$ are plotted against the momentum k in Fig. 10 when $\mathbf{q}=10k_F\mathbf{e}_\mathbf{y}$. In this case, due to the small density and hence small q, the unpairing regions mentioned in Sec. IV A are absent here. Moreover, as seen from the figure, the SE order parameter $\Delta_{\rm SE}$ (red solid curve) is efficiently suppressed, and as expected above, along the $\mathbf{e}_\mathbf{x}$ ($\mathbf{e}_\mathbf{y}$) direction with $\Delta_{\rm SO}=\Delta_{\rm TO}=0$ ($\Delta_{\rm TE}=\Delta_{\rm TO}=0$) the TE (SO) order parameter (blue long-dashed curve) [(green short-dashed curve)] is dominant, providing the possibility to distinguish this order parameter solely by detecting along special direction.

Nevertheless, as for the d_{xy}-wave TO order parameter at $\mathbf{q}=q\mathbf{e}_\mathbf{y}$, along the $\mathbf{e}_\mathbf{c}$ direction, the maximum of the strength of the TO order parameter (black chain curve) is comparable to that of the SO (gray double-dotted curve) and TE (light blue dotted curve) ones. However, with the experimentally obtained order parameter $\Delta^e(\mathbf{k},\omega)$, since the SE order parameter is suppressed at small density and the SO and TE ones can be obtained above, one obtains $\Delta_{\rm TO}(\mathbf{k},\omega)=\Delta^e(\mathbf{k},\omega)-\Delta_{\rm SO}(\mathbf{k},\omega)-\Delta_{\rm TE}(\mathbf{k},\omega)$ or

$$\Delta_{\rm TO}(\mathbf{k},\omega)=\int d\theta_\mathbf{k}\Delta^e(\mathbf{k},\omega)\sin\theta_\mathbf{k}\cos\theta_\mathbf{k}/(4\pi). \tag{38}$$

Then, the d_{xy}-wave TO order parameter can also be detected. Moreover, with the strength comparable to the SO one, the TO order parameter has been shown to provide significant protection to the zero-energy states including the Andreev bound state and Majorana fermion state due to the even parity [3], and promises to lead to rich physics [43,92,93] including the long-range proximity effect [43] and anomalous features of quasiparticle [92,93].

V. SUMMARY AND DISCUSSION

In summary, we have demonstrated that the SE, SO, TE, and TO pairings and the corresponding order parameters can be realized in spin-orbit-coupled InSb (110) QW in proximity to s-wave superconductor in FFLO phase or with a supercurrent. Specifically, the SE order parameter can be induced in QW through the proximity effect. Nevertheless, it is found that there exist unpairing regions in the momentum space, in which the proximity-induced SE order parameter vanishes. We further reveal that the unpairing regions arise from the FFLO-phase-like blocking in QW. In the presence of this proximity-induced SE order parameter, the SO pairing is induced due to the broken translational symmetry by the c.m. momentum of Cooper pair whereas the TE one is induced due to the broken spin-rotational symmetry by the SOC. Moreover, with the translational and spin-rotational asymmetries, the TO pairing is induced. Then, the corresponding order parameters can be induced from the self-energy of the e-e Coulomb interaction with the dynamic screening, and the proximity-induced SE order parameter is also renormalized. Particularly, we reveal that the odd-frequency order parameters are induced due to the retardation effect of the Coulomb interaction from the dynamic screening in 2DEG, where the plasmon effect is important.

Differing from the vanishing proximity-induced SE order parameter in the unpairing regions, we show that through the renormalization, the SE, SO, TE, and TO order parameters in QW all have small strengths in the unpairing regions. In the pairing regions, the SE and TE order parameters are revealed to show the conventional s- and p-wave characters, respectively. As for the odd-frequency order parameters, which are difficult to realize in bulk superconductors, the induced SO and TO order parameters in InSb (110) QW exhibit the p- and d-wave characters, respectively. Specifically, with the broken translational symmetry by the c.m. momentum of Cooper pair, the p-wave character of the SO order parameter shows anisotropy with respect to the direction of the c.m. momentum. This is very different from the TE one, which is determined by the SOC and hence is independent on the direction of the c.m. momentum. As for the unconventional d-wave TO order parameter, it is interesting to find that d_{x^2}- and d_{xy}-wave TO order parameters can be obtained when the c.m. momentum is along the $[1\bar{1}0]$ and [001] directions, respectively. It is further demonstrated that this anisotropy of the TO order parameter arises from the unique SOC structure in InSb (110) QW.

Furthermore, we show that at proper density, the SE order parameter can be efficiently suppressed. Then, the induced SO, TE, and TO order parameters can be detected experimentally. Our work provides an idea platform where rich physics, including the enhanced Josephson current [94], dispersionless zero-energy Andreev bound states [3,19,95–97], and anomalous proximity effect [3,98,99] related to the SO order parameter, the conventional triplet superconductivity [37–39,98–103] associated with the TE one, and the long-range proximity effect [43] and anomalous features of quasiparticle [92,93] due to the TO one can be realized.

ACKNOWLEDGMENTS

This work was supported by the National Natural Science Foundation of China under Grants No. 11334014 and No. 61411136001, and the Strategic Priority Research Program of the Chinese Academy of Sciences under Grant No. XDB01000000.

APPENDIX A: DERIVATION OF EQ. (20)

We derive Eq. (20) in this appendix. By neglecting the frequency dependence of the self-energy due to the proximity effect as mentioned in Sec. III B, Eq. (19) can be expressed as

$$\frac{\hat{\Delta}_T(\mathbf{k})}{\Delta_0} = \int_{|\varepsilon^s_{\mathbf{k}\pm\mathbf{q}}+\xi^s_{p_z}|<\omega_D} \frac{m^*_s d\varepsilon^s_{p_z}}{2\pi p_z} \begin{pmatrix} 0 & \frac{|t_0|^2}{\Xi^+_{\mathbf{k},p_z}} \\ \frac{|t_0|^2}{-\Xi^-_{\mathbf{k},p_z}} & 0 \end{pmatrix}, \quad \text{(A1)}$$

where ω_D represents the Debye frequency of superconductor and $\Xi^{\pm}_{\mathbf{k}}(\xi^s_{p_z}) = (\varepsilon^s_{\mathbf{k}+\mathbf{q}} + \xi^s_{p_z} \pm h_B)(\varepsilon^s_{\mathbf{k}-\mathbf{q}} + \xi^s_{p_z} \mp h_B) + |\Delta_0|^2$.

Moreover, with the small momentum $\mathbf{k}$ in QW, one has $\varepsilon^s_{\mathbf{k}} \ll \omega_D \ll \mu_s$ and hence the restriction $|\varepsilon^s_{\mathbf{k}\pm\mathbf{q}} + \xi^s_{p_z}| < \omega_D$ in the integral of Eq. (A1) can be approximated as $|\xi^s_{p_z}| < \omega_D$. Then, by using the mean value theorem for the integral in Eq. (A1), one gets

$$\hat{\Delta}_T(\mathbf{k}) = \frac{|t_0|^2 \Delta_0 \omega_D \sqrt{m^*_s}}{\pi\sqrt{2\mu_s}} \begin{pmatrix} 0 & \frac{1}{L^+_{\mathbf{k}}} \\ -\frac{1}{L^-_{\mathbf{k}}} & 0 \end{pmatrix}, \quad \text{(A2)}$$

with $L^{\pm}_{\mathbf{k}} = \varepsilon^s_{\mathbf{k}+\mathbf{q}}\varepsilon^s_{\mathbf{k}-\mathbf{q}} - h_B^2 + |\Delta_0|^2 \pm (\varepsilon^s_{\mathbf{k}+\mathbf{q}} - \varepsilon^s_{\mathbf{k}-\mathbf{q}})h_B$.

As mentioned in Sec. IV A, it is found that $|\Delta_0| \approx \varepsilon^s_{15k_F}$, and hence $(\varepsilon^s_{\mathbf{k}+\mathbf{q}} - \varepsilon^s_{\mathbf{k}-\mathbf{q}})$ in $L^{\pm}_{\mathbf{k}}$ can be neglected due to the small c.m. momentum q in this work. Then, Eq. (20) is obtained with the effective tunneling matrix element $|\tilde{t}|^2 = |t_0|^2\omega_D\sqrt{m^*_s/(2\mu_s)}/\pi$.

APPENDIX B: MOMENTUM DEPENDENCE OF THE DEPAIRING OPERATOR

In this Appendix, we show the momentum dependencies of the depairing operator $\delta_{\mathbf{k}}$ at different c.m. momenta, which are plotted in Fig. 11. We find that at $n = 5n_0$, when $q > 0.74k_F$, there always exist zero-value regions of the depairing operator in the momentum space (shown by the blue regions in Fig. 11 at $q = 0.8k_F$), which exactly correspond to the unpairing regions in Sec. IV A [blue regions in Figs. 1(c) and 1(d)].

Nevertheless, due to the existence of the SOC, there exist four unpairing regions in the momentum space at fixed $\mathbf{q}$ when $q > 0.74k_F$. This is very different from the conventional FFLO

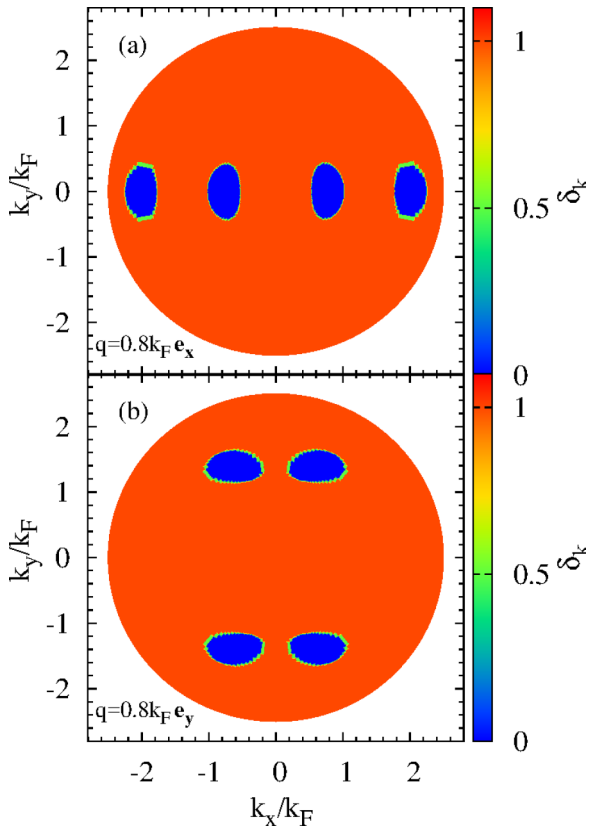

FIG. 11. Momentum dependence of the depairing operator at (a) $\mathbf{q} = 0.8k_F\mathbf{e}_\mathbf{x}$ and (b) $\mathbf{q} = 0.8k_F\mathbf{e}_\mathbf{y}$. $n = 5n_0$.

superconductor [72,73], where only two unpairing regions exist. This can also be understood from the four nondegenerate quasiparticle energy spectra addressed in Sec. III A, differing from the two double-degenerate quasiparticle energy spectra in the conventional FFLO superconductors [72,73].

APPENDIX C: DERIVATION OF EQS. (27), (29), (33), AND (36)

We derive Eqs. (27), (29), (33), and (36) in this appendix. Specifically, at low temperature, one has $f(E^{\mu}_{\nu\mathbf{k}}) \approx 0$ since $E^{\mu}_{\nu\mathbf{k}} > 0$ and $n(\omega^{pl}_{\mathbf{k}})\omega^{pl}_{\mathbf{k}} \approx 0$, so the second and the third terms in Eq. (24) can be neglected. Moreover, since the Coulomb interaction $V^0_{\mathbf{k}-\mathbf{k}'}$ is very strong at $\mathbf{k}' = \mathbf{k}$, the plasma frequency $\omega^{pl}_{\mathbf{k}-\mathbf{k}'} \propto \sqrt{|\mathbf{k}-\mathbf{k}'|}$ in the denominator of the first term can also be neglected (compared with $E^{\mu}_{\nu\mathbf{k}'}$). Then, the renormalization-induced singlet order parameter [Eq. (24)] is simplified into

$$\Delta_s(\mathbf{k},\omega) = \sum_{\mu=\pm}\int \frac{d\mathbf{k}'}{32\pi^2} V^0_{\mathbf{k}-\mathbf{k}'}\Delta^T_{\mathrm{SE}}\left(\frac{\omega^{pl}_{\mathbf{k}-\mathbf{k}'}}{A^{\mu+}_{\mathbf{k}'}} - \frac{1}{B^{\mu}_{+\mathbf{k}'}}\right), \quad \text{(C1)}$$

where $A^{\mu\nu}_{\mathbf{k}'} = E^{\mu}_{+\mathbf{k}'}E^{\mu}_{-\mathbf{k}'} - \omega^2 + \nu\omega B^{\mu}_{-\mathbf{k}'}$ and $B^{\mu}_{\pm\mathbf{k}'} = E^{\mu}_{+\mathbf{k}'} \pm E^{\mu}_{-\mathbf{k}'}$.

Then, the renormalization-induced SE order parameter and SO one can be obtained from Eqs. (26) and (28), respectively, written as

$$\Delta^R_{\mathrm{SE}}(\mathbf{k},\omega) = \sum_{\nu,\mu=\pm}\int \frac{d\mathbf{k}'}{64\pi^2} V^0_{\mathbf{k}-\mathbf{k}'}\Delta^T_{\mathrm{SE}}\left(\frac{\omega^{pl}_{\mathbf{k}-\mathbf{k}'}}{A^{\mu\nu}_{\mathbf{k}'}} - \frac{1}{B^{\mu}_{+\mathbf{k}'}}\right), \quad \text{(C2)}$$

$$\Delta_{\mathrm{SO}}(\mathbf{k},\omega) = \sum_{\nu,\mu=\pm}\nu\int \frac{d\mathbf{k}'}{64\pi^2} \frac{V^0_{\mathbf{k}-\mathbf{k}'}\Delta^T_{\mathrm{SE}}\omega^{pl}_{\mathbf{k}-\mathbf{k}'}}{A^{\mu\nu}_{\mathbf{k}'}}. \quad \text{(C3)}$$

By approximately considering ω, $\varepsilon^c_{\mathbf{q}}$, and $h_{\mathbf{k}'}$ as small quantities (compared with $\xi^c_{\mathbf{k}'}$ and Δ^T_{SE}) for expansion, Eq. (C2) [Eq. (C3)] can be further simplified, and then Eq. (27) [Eq. (29)] can be obtained.

Similarly, by taking the same approximation $n(\omega^{pl}_{\mathbf{k}})\omega^{pl}_{\mathbf{k}} \approx 0$ and $f(E^{\mu}_{\nu\mathbf{k}}) \approx 0$ at low temperature and $\omega^{pl}_{\mathbf{k}-\mathbf{k}'} < E^{\mu}_{\nu\mathbf{k}'}$ in Eq. (25), the induced TE order parameter and TO one can be

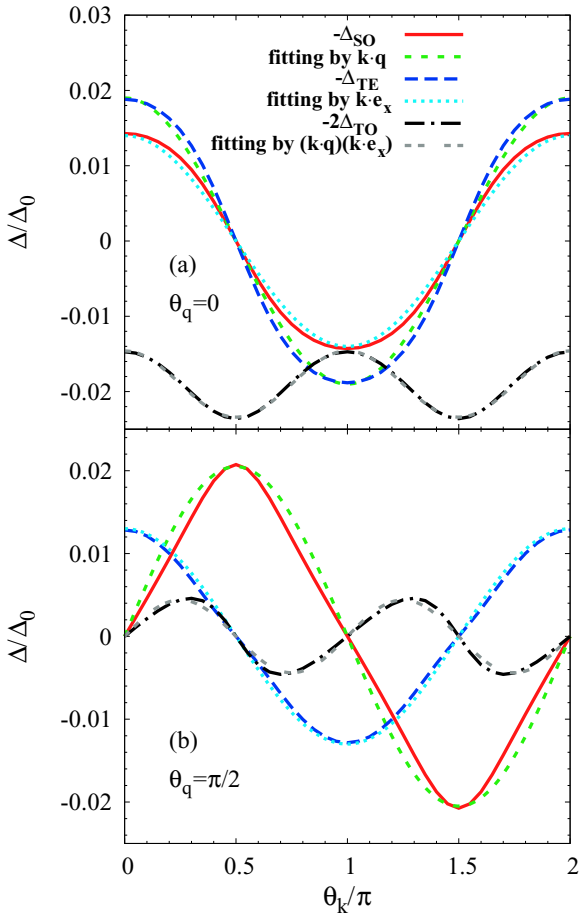

FIG. 12. Momentum-orientation dependence of the order parameters at (a) $\mathbf{q} = 0.4k_F\mathbf{e}_\mathbf{x}$ and (b) $\mathbf{q} = 0.4k_F\mathbf{e}_\mathbf{y}$. $n = 5n_0$. $\omega = E_F$ and $k = k_F$. Red solid, blue long-dashed, and black chain curves denote the full numerical results of the SO, TE, and TO order parameters, respectively. Green short-dashed curve (light blue dotted curve): fitted results for the SO (TE) order parameter by using $\Delta_{\mathrm{SO}} = C_{\mathrm{SO}}(k,\omega)\mathbf{k}\cdot\mathbf{q}$ [$\Delta_{\mathrm{TE}} = C_{\mathrm{TE}}(k,\omega)\mathbf{k}\cdot\mathbf{e}_\mathbf{x}$]. Gray double-dotted curve: fitted results for the TO one by using $\Delta_{\mathrm{TO}} = C^0_{\mathrm{TO}}(k,\omega) - C^1_{\mathrm{TO}}(k,\omega)(\mathbf{k}\cdot\mathbf{e}_\mathbf{x})(\mathbf{k}\cdot\mathbf{q})$.

obtained from Eqs. (32) and (35), respectively, written as

$$\Delta_{\rm TE}(\mathbf{k},\omega)=\sum_{\nu,\mu=\pm}\mu\int\frac{d\mathbf{k}'}{64\pi^2}V^0_{\mathbf{k}-\mathbf{k}'}\Delta^T_{\rm SE}\left(\frac{\omega^{pl}_{\mathbf{k}-\mathbf{k}'}}{A^{\mu\nu}_{\mathbf{k}'}}-\frac{1}{B^{\mu}_{+\mathbf{k}'}}\right), \tag{C4}$$

$$\Delta_{\rm TO}(\mathbf{k},\omega)\sum_{\nu,\mu=\pm}\mu\nu\int\frac{d\mathbf{k}'}{64\pi^2}\frac{V^0_{\mathbf{k}-\mathbf{k}'}\Delta^T_{\rm SE}\omega^{pl}_{\mathbf{k}-\mathbf{k}'}}{A^{\mu\nu}_{\mathbf{k}'}}. \tag{C5}$$

Then, by further approximately taking ω, $\varepsilon^c_{\mathbf{q}}$, and $h_{\mathbf{k}'}$ as small quantities, Eq. (C4) [Eq. (C4)] is simplified into Eq. (33) [Eq. (36)].

APPENDIX D: MOMENTUM-ORIENTATION DEPENDENCE OF ORDER PARAMETERS

In this Appendix, we show the momentum-orientation dependencies of the four order parameters at different c.m. momenta, which are plotted in Fig. 12 at $n=5n_0$. As seen from the figure, the full numerical results of the SO (red solid curve), TE (light blue dotted curve), and TO (gray double-dotted curve) order parameters can be well fitted by using the analytic analyses addressed in Table I: $\Delta_{\rm SO}=C_{\rm SO}(k,\omega)\mathbf{k}\cdot\mathbf{q}$ (green short-dashed curve), $\Delta_{\rm TE}=C_{\rm TE}(k,\omega)\mathbf{k}\cdot\mathbf{e_x}$ (blue long-dashed curve), and $\Delta_{\rm TO}=C^0_{\rm TO}(k,\omega)-C^1_{\rm TO}(k,\omega)(\mathbf{k}\cdot\mathbf{e_x})(\mathbf{k}\cdot\mathbf{q})$ (black chain curve), respectively.

APPENDIX E: DENSITY DEPENDENCIES OF THE ORDER PARAMETERS CONTAINING ALL FOUR TYPES

1. Density dependence of the renormalization-induced SE order parameter

We first address the density dependence of the renormalization-induced SE order parameter. The strengths of the renormalization-induced SE order parameter $-\Delta^R_{\rm SE}(\mathbf{k}=0,\omega)$ versus density n when $\mathbf{q}=0.4k_F\mathbf{e_x}$ are plotted in Fig. 13 at different frequencies ω. As shown from the figure,

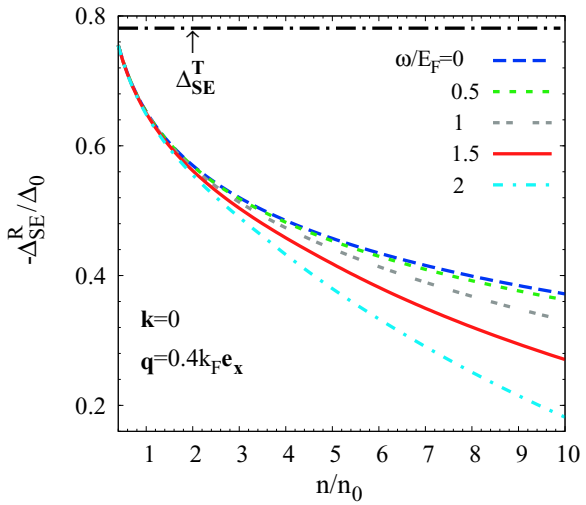

FIG. 13. Strength of the renormalization-induced SE order parameter $|\Delta^R_{\rm SE}(\mathbf{k}=\mathbf{0},\omega)|=-\Delta^R_{\rm SE}(\mathbf{k}=\mathbf{0},\omega)$ versus density n at different frequencies ω. Black chain line: results for $\Delta^T_{\rm SE}$. $\mathbf{q}=0.4k_F\mathbf{e_x}$.

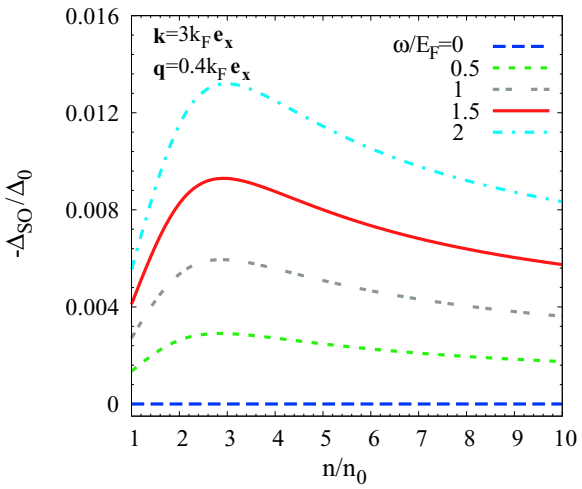

FIG. 14. Strength of the SO order parameter $|\Delta_{\rm SO}(\mathbf{k}=3k_F\mathbf{e_x},\omega)|=-\Delta_{\rm SO}(\mathbf{k}=3k_F\mathbf{e_x},\omega)$ versus density n at different frequencies. $\mathbf{q}=0.4k_F\mathbf{e_x}$.

$-\Delta^R_{\rm SE}(\mathbf{k}=0,\omega)$ decreases monotonically with the increase of the density. This behavior can also be understood from Eq. (27). The vanishing renormalization-induced SE order parameter at large density comes from the vanishing pairing function at $|\xi^c_{k=0}|\gg\Delta^T_{\rm SE}$ as mentioned above, similar to the case at large momentum. At small density, the attractive potential $V^{\rm at}_{\mathbf{k}}$ is efficiently suppressed, leading to the enhanced Coulomb interaction and hence the renormalization-induced SE order parameter.

Furthermore, it is noted that with the decrease of the density, the strength of the renormalization-induced SE order parameter $-\Delta^R_{\rm SE}$ becomes close to that of the proximity-induced one $\Delta^T_{\rm SE}$ (black chain line). Since $\Delta^R_{\rm SE}$ is always in the opposite sign against $\Delta^T_{\rm SE}$, the SE order parameter $\Delta_{\rm SE}=\Delta^T_{\rm SE}+\Delta^R_{\rm SE}$ in QW can be efficiently suppressed, providing the possibility for the experimental observation for SO, TE, and TO ones, as mentioned in Sec. IV E.

Additionally, from Fig. 13, it is found that at fixed density, the strength of the renormalization-induced SE order parameter $-\Delta^R_{\rm SE}(\mathbf{k}=0,\omega)$ decreases monotonically with the increase of the frequency, in accord with the analytic results in Eq. (27).

2. Density dependence of the SO order parameter

We next address the density dependence of the SO order parameter. The strengths of the SO order parameter $|\Delta_{\rm SO}(\mathbf{k}=3k_F\mathbf{e_x},\omega)|$ as function of the density n are plotted in Fig. 14 at different frequencies when $\mathbf{q}=0.4k_F\mathbf{e_x}$. As seen from the figure, with the increase of the density n, $|\Delta_{\rm SO}(\mathbf{k}=3k_F\mathbf{e_x},\omega)|$ first increases when $n<2.8n_0$ then decreases when $n>2.8n_0$, leading to a peak around $2.8n_0$.

The peak behavior can be understood as follows. At small (large) density with $\xi_{3k_F}\ll\Delta^T_{\rm SE}$ ($\xi_{3k_F}\gg\Delta^T_{\rm SE}$), the strength for the SO order parameter is enhanced (suppressed) due to the enhanced effective attractive potential $V^{\rm at}_{\mathbf{k}}\propto|\omega^{pl}_{\mathbf{k}}|^2\propto n$ (suppressed pairing potential as mentioned in Sec. IV A), and then a density peak of the strength for the SO order parameter is expected. This can also be understood from Eq. (29). By

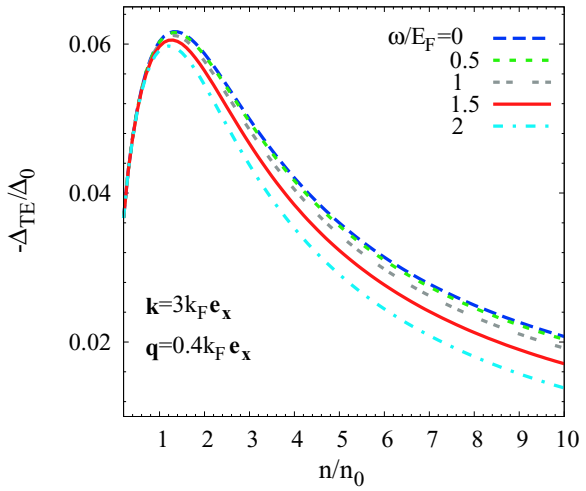

FIG. 15. Strength of the TE order parameter $|\Delta_{\rm TE}(\mathbf{k}=3k_F\mathbf{e}_\mathbf{x},\omega)| = -\Delta_{\rm TE}(\mathbf{k}=3k_F\mathbf{e}_\mathbf{x},\omega)$ versus density n at different frequencies. $\mathbf{q}=0.4k_F\mathbf{e}_\mathbf{x}$.

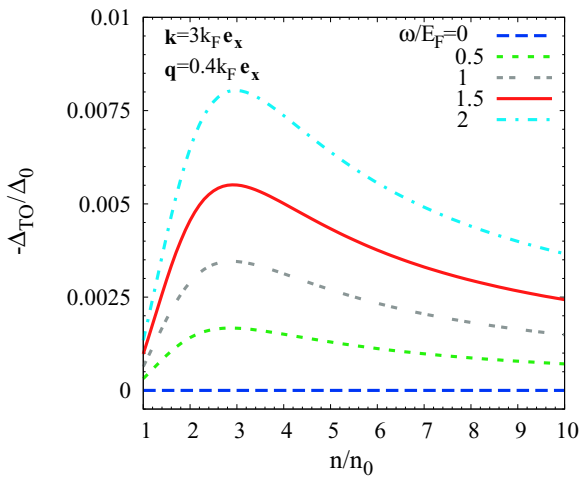

FIG. 16. Strength of the TO order parameter $|\Delta_{\rm TO}(\mathbf{k}=3k_F\mathbf{e}_\mathbf{x},\omega)| = -\Delta_{\rm TO}(\mathbf{k}=3k_F\mathbf{e}_\mathbf{x},\omega)$ versus density n at different frequencies when $\mathbf{q}=0.4k_F\mathbf{e}_\mathbf{x}$.

approximately taking the Coulomb interaction $V^0_{\mathbf{k}-\mathbf{k}'}\omega^{pl}_{\mathbf{k}-\mathbf{k}'}$ as a delta function, it is found $|\Delta_{\rm SO}(\mathbf{k}=3k_F\mathbf{e}_\mathbf{x},\omega)| \propto \sqrt{nE_F}E_F/(8E_F^2+|\Delta^T_{\rm SE}|^2)^2$, showing peak behavior in the density dependence.

Moreover, from Fig. 14, it is found that at fixed density, the strength of the SO order parameter $|\Delta_{\rm SO}(\mathbf{k}=3k_F\mathbf{e}_\mathbf{x},\omega)|$ increases with the frequency, in accord with the analytic results in Eq. (29).

3. Density dependence of the TE order parameter

We next address the density dependence of the TE order parameter. The strengths of TE order parameters $|\Delta_{\rm TE}(\mathbf{k}=3k_F\mathbf{e}_\mathbf{x},\omega)|$ versus the density n are plotted in Fig. 15 at different frequencies. As shown from the figure, with the increase of the density, $|\Delta_{\rm TE}(\mathbf{k}=3k_F\mathbf{e}_\mathbf{x},\omega)|$ first increases when $n<1.2n_0$ then decreases after $n>1.2n_0$, leading to a peak around $1.2n_0$, similar to the results of the SO order parameter.

The density dependence of $|\Delta_{\rm TE}(\mathbf{k}=3k_F\mathbf{e}_\mathbf{x},\omega)|$ can be understood from the momentum-magnitude dependence since the increase of the density leads to the increase of $3k_F$. Then, the density dependence shows similar behavior of the momentum-magnitude dependence, and the density peak (shown in Fig. 15) corresponds to the momentum-magnitude peak above (shown in Fig. 7).

In addition, we also find that at fixed density, the strength of the TE order parameter $-\Delta_{\rm TE}(\mathbf{k}=3k_F\mathbf{e}_\mathbf{x},\omega)$ decreases with the increases of the frequency, as shown in Fig. 15, in good agreement with Eq. (33).

4. Density dependence of the TO order parameter

We then address the density dependence of the TO order parameter. The strengths of TO order parameter are plotted against the density n in Fig. 16 at different frequencies. As shown from the figure, with the increase of the density, a peak is observed in the density dependence of $\Delta_{\rm TO}(\mathbf{k}=3k_F\mathbf{e}_\mathbf{x},\omega)$, similar to the previous results of the SO and TE order parameters.

With the similar analysis for the density dependence of the SO and TE order parameter, the strength for the TO one is enhanced (suppressed) by the increase of the density at small (large) density due to the enhanced effective attractive potential $V^{\rm at}_\mathbf{k}$ and SOC $h_{3k_F\mathbf{e}_\mathbf{x}}$ (suppressed pairing potential as mentioned in Sec. IV A), leading to a peak observed.

Moreover, from Fig. 16, it is found that at fixed density, the strength of the TO order parameter $|\Delta_{\rm TO}|$ increases with the frequency, in accord with the analytic results in Eq. (36).

[1] J. Bardeen, L. N. Cooper, and J. R. Schrieffer, Phys. Rev. **106**, 162 (1957).
[2] V. L. Berezinskii, Pis'ma Zh. Eksp. Teor. Fiz. **20**, 628 (1974) [JETP Lett. **20**, 287 (1974)].
[3] Y. Tacdrinaka, M. Sato, and N. Nagaosa, J. Phys. Soc. Jpn. **81**, 011013 (2012).
[4] P. Coleman, E. Miranda, and A. Tsvelik, Phys. Rev. Lett. **70**, 2960 (1993).
[5] N. Bulut, D. J. Scalapino, and S. R. White, Phys. Rev. B **47**, 14599 (1993).
[6] P. Coleman, E. Miranda, and A. Tsvelik, Phys. Rev. B **49**, 8955 (1994).
[7] M. Vojta and E. Dagotto, Phys. Rev. B **59**, R713 (1999).
[8] K. Shigeta, Y. Tanaka, K. Kuroki, S. Onari, and H. Aizawa, Phys. Rev. B **83**, 140509 (2011).
[9] H. Kusunose, Y. Fuseya, and K. Miyake, J. Phys. Soc. Jpn. **80**, 044711 (2011).
[10] H. Kusunose, Y. Fuseya, and K. Miyake, J. Phys. Soc. Jpn. **80**, 054702 (2011).
[11] T. Hotta, J. Phys. Soc. Jpn. **78**, 123710 (2009).
[12] A. Balatsky and E. Abrahams, Phys. Rev. B **45**, 13125 (1992).
[13] E. Abrahams, A. Balatsky, J. R. Schrieffer, and P. B. Allen, Phys. Rev. B **47**, 513 (1993).

[14] P. Coleman, A. Georges, and A. M. Tsvelik, J. Phys.: Condens. Matter **9**, 345 (1997).
[15] Y. Fuseya, H. Kohno, and K. Miyake, J. Phys. Soc. Jpn. **72**, 2914 (2003).
[16] K. Shigeta, S. Onari, K. Yada, and Y. Tanaka, Phys. Rev. B **79**, 174507 (2009).
[17] E. Abrahams, A. Balatsky, D. J. Scalapino, and J. R. Schrieffer, Phys. Rev. B **52**, 1271 (1995).
[18] V. Ambegaokar, P. G. de Gennes, and D. Rainer, Phys. Rev. A **9**, 2676 (1974).
[19] L. J. Buchholtz and G. Zwicknagl, Phys. Rev. B **23**, 5788 (1981).
[20] Y. Nagato, M. Yamamoto, and K. Nagai, J. Low Temp. Phys. **110**, 1135 (1998).
[21] Y. Aoki, Y. Wada, M. Saitoh, R. Nomura, Y. Okuda, Y. Nagato, M. Yamamoto, S. Higashitani, and K. Nagai, Phys. Rev. Lett. **95**, 075301 (2005).
[22] S. Murakawa, Y. Tamura, Y. Wada, M. Wasai, M. Saitoh, Y. Aoki, R. Nomura, Y. Okuda, Y. Nagato, M. Yamamoto, S. Higashitani, and K. Nagai, Phys. Rev. Lett. **103**, 155301 (2009).
[23] S. Murakawa, Y. Wada, Y. Tamura, M. Wasai, M. Saitoh, Y. Aoki, R. Nomura, Y. Okuda, Y. Nagato, M. Yamamoto, S. Higashitani, and K. Nagai, J. Phys. Soc. Jpn. **80**, 013602 (2011).
[24] K. Nagai, Y. Nagato, M. Yamamoto, and S. Higashitani, J. Phys. Soc. Jpn. **77**, 111003 (2008).
[25] S. Higashitani, Y. Nagato, and K. Nagai, J. Low Temp. Phys. **155**, 83 (2009).
[26] A. Layzer and D. Fay, Int. J. Magn. **1**, 135 (1971).
[27] P. W. Anderson and W. F. Brinkman, Phys. Rev. Lett. **30**, 1108 (1973).
[28] W. F. Brinkman, J. W. Serene, and P. W. Anderson, Phys. Rev. A **10**, 2386 (1974).
[29] Y. Maeno, H. Hashimoto, K. Yoshida, S. Nishizaki, T. Fujita, J. G. Bednorz, and F. Lichtenberg, Nature (London) **372**, 532 (1994).
[30] T. M. Rice and M. Sigrist, J. Phys.: Condens. Matter **7**, L643 (1995).
[31] K. Ishida, Y. Kitaoka, K. Asayama, S. Ikeda, S. Nishizaki, Y. Maeno, K. Yoshida, and T. Fujita, Phys. Rev. B **56**, R505(R) (1997).
[32] N. Read and D. Green, Phys. Rev. B **61**, 10267 (2000).
[33] D. A. Ivanov, Phys. Rev. Lett. **86**, 268 (2001).
[34] A. P. Mackenzie and Y. Maeno, Rev. Mod. Phys. **75**, 657 (2003).
[35] V. M. Edelstein, Phys. Rev. B **67**, 020505(R) (2003).
[36] I. Eremin, D. Manske, S. G. Ovchinnikov, and J. F. Annett, Ann. Phys. (NY) **13**, 149 (2004).
[37] M. Sigrist and K. Ueda, Rev. Mod. Phys. **63**, 239 (1991).
[38] P. A. Frigeri, D. F. Agterberg, A. Koga, and M. Sigrist, Phys. Rev. Lett. **92**, 097001 (2004).
[39] E. Bauer and M. Sigrist, *Non-centrosymmetric Superconductors: Introduction and Overview* (Springer, Berlin, 2012).
[40] G. Dresselhaus, Phys. Rev. **100**, 580 (1955).
[41] Y. A. Bychkov and E. I. Rashba, J. Phys. C: Solid State Phys. **17**, 6039 (1984).
[42] Y. A. Bychkov, Pis'ma Zh. Eksp. Teor. Fiz. **39**, 66 (1984) [JETP Lett. **39**, 78 (1984)].
[43] F. S. Bergeret, A. F. Volkov, and K. B. Efetov, Phys. Rev. Lett. **86**, 4096 (2001).
[44] A. I. Buzdin, Rev. Mod. Phys. **77**, 935 (2005).
[45] Y. Tanaka and A. A. Golubov, Phys. Rev. Lett. **98**, 037003 (2007).
[46] Y. Tanaka, A. A. Golubov, S. Kashiwaya, and M. Ueda, Phys. Rev. Lett. **99**, 037005 (2007).
[47] Y. Tanaka, Y. Tanuma, and A. A. Golubov, Phys. Rev. B **76**, 054522 (2007).
[48] M. Eschrig, T. Löfwander, T. Champel, J. Cuevas, and G. Schön, J. Low Temp. Phys. **147**, 457 (2007).
[49] F. S. Bergeret and I. V. Tokatly, Phys. Rev. Lett. **110**, 117003 (2013); Phys. Rev. B **89**, 134517 (2014).
[50] A. D. Bernardo, S. Diesch, Y. Gu, J. Linder, G. Divitini, C. Ducati, E. Scheer, M. G. Blamire, and J. W. A. Robinson, Nat. Commun. **6**, 8053 (2015).
[51] Y. Kalcheim, O. Millo, A. DiBernardo, A. Pal, and J. W. A. Robinson, Phys. Rev. B **92**, 060501(R) (2015).
[52] L. P. Gor'kov and E. I. Rashba, Phys. Rev. Lett. **87**, 037004 (2001).
[53] Z. H. Yang, J. Wang, and K. S. Chan, Supercond. Sci. Technol. **22**, 055012 (2009).
[54] X. Liu, J. K. Jain, and C. X. Liu, Phys. Rev. Lett. **113**, 227002 (2014).
[55] C. R. Reeg and D. L. Maslov, Phys. Rev. B **92**, 134512 (2015).
[56] C. Triola, D. M. Badiane, A. V. Balatsky, and E. Rossi, Phys. Rev. Lett. **116**, 257001 (2016).
[57] S. H. Jacobsen, I. Kulagina, and J. Linder, Sci. Rep. **6**, 23926 (2016).
[58] T. Yu and M. W. Wu, Phys. Rev. B **93**, 195308 (2016).
[59] P. G. de Gennes, Rev. Mod. Phys. **36**, 225 (1964).
[60] C. Caroli, P. G. de Gennes, and J. Matricon, Phys. Lett. **9**, 307 (1964).
[61] H. F. Hess, R. B. Robinson, R. C. Dynes, J. M. Valles, and J. V. Waszczak, Phys. Rev. Lett. **62**, 214 (1989).
[62] F. Gygi and M. Schlüter, Phys. Rev. B **43**, 7609 (1991).
[63] Y. G. Makhlin and G. E. Volovik, JETP Lett. **62**, 737 (1995).
[64] N. B. Kopnin and G. E. Volovik, Phys. Rev. Lett. **79**, 1377 (1997).
[65] N. Hayashi, T. Isoshima, M. Ichioka, and K. Machida, Phys. Rev. Lett. **80**, 2921 (1998).
[66] A. I. Larkin and Y. N. Ovchinnikov, Phys. Rev. B **57**, 5457 (1998).
[67] G. E. Volovik, JETP Lett. **70**, 609 (1999).
[68] T. Yokoyama, Y. Tanaka, and A. A. Golubov, Phys. Rev. B **78**, 012508 (2008).
[69] Y. Tanuma, N. Hayashi, Y. Tanaka, and A. A. Golubov, Phys. Rev. Lett. **102**, 117003 (2009).
[70] F. Rohlfing, G. Tkachov, F. Otto, K. Richter, D. Weiss, G. Borghs, and C. Strunk, Phys. Rev. B **80**, 220507 (2009).
[71] T. Yu and M. W. Wu, Phys. Rev. B **94**, 205305 (2016).
[72] P. Fulde and A. Ferrell, Phys. Rev. **135**, A550 (1964).
[73] A. I. Larkin and Y. N. Ovchinnikov, Sov. Phys.–JETP **20**, 762 (1965).
[74] C. F. Chan and M. Gong, Phys. Rev. B **89**, 174501 (2014).
[75] H. Takayanagi and T. Kawakami, Phys. Rev. Lett. **54**, 2449 (1985).
[76] T. Akazaki, H. Takayanagi, J. Nitta, and T. Enoki, Appl. Phys. Lett. **68**, 418 (1996).
[77] K. M. H. Lenssen, M. Matters, C. J. P. M. Harmans, J. E. Mooij, M. R. Leys, W. van der Vleuten, and J. H. Wolter, Appl. Phys. Lett. **63**, 2079 (1993).
[78] T. D. Moore and D. A. Williams, Phys. Rev. B **59**, 7308 (1999).

[79] Z. Wan, A. Kazakov, M. J. Manfra, L. N. Pfeiffer, K. W. West, and L. P. Rokhinson, Nat. Commun. **6**, 7426 (2015).
[80] A. A. Abrikosov, L. P. Gorkov, and I. E. Dzyaloshinski, *Methods of Quantum Field Theory in Statistical Physics* (Prentice Hall, Englewood Cliffs, NJ, 1963).
[81] A. L. Fetter and J. D. Walecka, *Quantum Theory of Many Particle Systems* (McGraw-Hill, New York, 1971).
[82] G. D. Mahan, *Many Particle Physics* (Plenum, New York, 1990).
[83] J. Ruhman and P. A. Lee, Phys. Rev. B **94**, 224515 (2016).
[84] T. D. Stanescu, R. M. Lutchyn, and S. Das Sarma, Phys. Rev. B **84**, 144522 (2011).
[85] H. Y. Hui, P. M. R. Brydon, J. D. Sau, S. Tewari, and S. Das Sarma, Sci. Rep. **5**, 8880 (2015).
[86] J. Danon and K. Flensberg, Phys. Rev. B **91**, 165425 (2015).
[87] A. N. Chantis, M. van Schilfgaarde, and T. Kotani, Phys. Rev. Lett. **96**, 086405 (2006).
[88] L. P. Gor'kov, Zh. Eksp. Teor. Fiz. **36**, 1918 (1959) [Sov. Phys. JETP **9**, 1364 (1959)]; Zh. Eksp. Teor. Fiz. **37**, 1407 (1959) [Sov. Phys. JETP **10**, 998 (1960)].
[89] *Semiconductors*, edited by O. Madelung, Landolt-Börnstein, New Series Vol. 17a (Springer, Berlin, 1987).
[90] J.-M. Jancu, R. Scholz, E. A. de Andrada e Silva, and G. C. La Rocca, Phys. Rev. B **72**, 193201 (2005).
[91] W. Martienssen and H. Warlimont, *Springer Handbook of Condensed Matter and Materials Data*, Bd. 1 (Springer, New York, 2005).
[92] T. Yokoyama, Y. Tanaka, and A. A. Golubov, Phys. Rev. B **72**, 052512 (2005).
[93] T. Yokoyama, Y. Tanaka, and A. A. Golubov, Phys. Rev. B **75**, 134510 (2007).
[94] Y. Asano, Y. Tanaka, and S. Kashiwaya, Phys. Rev. Lett. **96**, 097007 (2006).
[95] J. Hara and K. Nagai, Prog. Theor. Phys. **76**, 1237 (1986).
[96] S. Kashiwaya and Y. Tanaka, Rep. Prog. Phys. **63**, 1641 (2000).
[97] T. Löfwander, V. S. Shumeiko, and G. Wendin, Supercond. Sci. Technol. **14**, R53 (2001).
[98] W. L. McMillan, Phys. Rev. **175**, 537 (1968).
[99] J. M. Rowell and W. L. McMillan, Phys. Rev. Lett. **16**, 453 (1966).
[100] Y. Tanaka and S. Kashiwaya, Phys. Rev. B **70**, 012507 (2004).
[101] Y. Tanaka, S. Kashiwaya, and T. Yokoyama, Phys. Rev. B **71**, 094513 (2005).
[102] J. Linder, Y. Tanaka, T. Yokoyama, A. Sudbo, and N. Nagaosa, Phys. Rev. Lett. **104**, 067001 (2010).
[103] J. Linder, Y. Tanaka, T. Yokoyama, A. Sudbo, and N. Nagaosa, Phys. Rev. B **81**, 184525 (2010).